Inorganic Chemistry
Article

Inorg. Chem. **2010**, *49*, 11333–11345 **11333**
DOI: 10.1021/ic1011617

Modulating the Light Switch by ^{3}MLCT-$^3\pi\pi^*$ State Interconversion

Brigitte R. Spencer, Brian J. Kraft, Chris G. Hughes, Maren Pink, and Jeffrey M. Zaleski*

Department of Chemistry and Molecular Structure Center, Indiana University, Bloomington, Indiana 47405, United States

Received June 9, 2010

The spectroscopic, electronic, and DNA-binding characteristics of two novel ruthenium complexes based on the dialkynyl ligands 2,3-bis(phenylethynyl)-1,4,8,9-tetraaza-triphenylene (bptt, **1**) and 2,3-bis(4-*tert*-butyl-phenylethynyl)-1,4,8,9-tetra-aza-triphenylene (tbptt, **2**) have been investigated. Electronic structure calculations of bptt reveal that the frontier molecular orbitals are localized on the pyrazine-dialkynyl portion of the free ligand, a property that is reflected in a red shift of the lowest energy electronic transition (**1**: λ_{max} = 393 nm) upon substitution at the terminal phenyl groups (**2**: λ_{max} = 398 nm). Upon coordination to ruthenium, the low-energy ligand-centered transitions of **1** and **2** are retained, and metal-to-ligand charge transfer transitions (MLCT) centered at λ_{max} = 450 nm are observed for $[Ru(phen)_2bptt]^{2+}$(**3**) and $[Ru(phen)_2tbptt]^{2+}$(**4**). The photophysical characteristics of **3** and **4** in ethanol closely parallel those observed for $[Ru(bpy)_3]^{2+}$ and $[Ru(phen)_3]^{2+}$, indicating that the MLCT excited state is primarily localized within the $[Ru(phen)_3]^{2+}$ manifold of **3** and **4**, and is only sparingly affected by the extended conjugation of the bptt framework. In an aqueous environment, **3** and **4** possess notably small luminescence quantum yields (**3**: ϕ_{H_2O} = 0.005, **4**: ϕ_{H_2O} = 0.011) and biexponential decay kinetics (**3**: τ_1 = 40 ns, τ_2 = 230 ns; **4**: $\tau_1 \sim$ 26 ns, τ_2 = 150 ns). Addition of CT-DNA to an aqueous solution of **3** causes a significant increase in the luminescence quantum yield (ϕ_{DNA} = 0.045), while the quantum yield of **4** is relatively unaffected (ϕ_{DNA} = 0.013). The differential behavior demonstrates that *tert*-butyl substitution on the terminal phenyl groups inhibits the ability of **4** to intercalate with DNA. Such changes in intrinsic luminescence demonstrate that **3** binds to DNA via intercalation ($K_b = 3.3 \times 10^4$ M^{-1}). The origin of this light switch behavior involves two competing ^{3}MLCT states similar to that of the extensively studied light switch molecule $[Ru(phen)_2dppz]^{2+}$. The solvent- and temperature-dependence of the luminescence of **3** reveal that the extended ligand aromaticity lowers the energy of the $^3\pi\pi^*$ excited state into competition with the emitting ^{3}MLCT state. Interconversion between these two states plays a significant role in the observed photophysics and is responsible for the dual emission in aqueous environments.

Introduction

Genotoxic agents including carcinogens or radiation exposure can cause DNA defects such as base pair mismatches and abasic sites that can lead to permanent mutations and disruption of transcription if not properly repaired.[1-4] If the genes that code for the repair machinery are themselves damaged and can no longer carry out their critical function, mutations can develop and accumulate leading to diseases such as cancer.[4-6] Therefore, a great deal of interest lies in metallo-insertors and metallo-intercalators that can interact intimately with DNA base pairs upon binding, and therefore can be structurally tuned to target these specific DNA defects or even particular DNA sequences.[7]

Metallo-intercalators (e.g., $[Ru(phen)_2dppz]^{2+}$, $[Ru(phen)_3]^{2+}$, $[Cu(bpod)_2]^{2+}$, and $[Pt(terpy)Cl]^+$)[8-14] bind between adjacent base pairs accompanied by a slight unwinding of the DNA helix for steric accommodation. In the case of insertion, the ligand is generally more sterically hindered, so to bind, a base pair must be ejected from the interior of the DNA helix. Therefore, metallo-insertors such as $[Rh(bpy)_2(chrysi)]^{3+}$

---

*To whom correspondence should be addressed. E-mail: zaleski@indiana.edu.

(1) Modrich, P. *Annu. Rev. Genet*. **1991**, *25*, 229–253.
(2) Kolodner, R. *Genes Dev*. **1996**, *10*, 1433–1442.
(3) Syvaenen, A.-C. *Nat. Rev. Genet*. **2001**, *2*, 930–942.
(4) David, S. S.; O'Shea, V. L.; Kundu, S. *Nature* **2007**, *447*, 941–950.
(5) Kolodner, R. D. *Trends Biochem. Sci*. **1995**, *20*, 397–401.
(6) Arzimanoglou, I. I.; Gilbert, F.; Barber, H. R. *Cancer* **1998**, *82*, 1808–1820.
(7) Zeglis, B. M.; Pierre, V. C.; Barton, J. K. *Chem. Commun*. **2007**, 4565–4579.
(8) Howe-Grant, M.; Wu, K. C.; Bauer, W. R.; Lippard, S. J. *Biochemistry* **1976**, *15*, 4339–4346.
(9) Friedman, A. E.; Chambron, J. C.; Sauvage, J. P.; Turro, N. J.; Barton, J. K. *J. Am. Chem. Soc*. **1990**, *112*, 4960–4862.
(10) Veal, J. M.; Rill, R. L. *Biochemistry* **1988**, *27*, 1822–1827.
(11) Veal, J. M.; Rill, R. L. *Biochemistry* **1989**, *28*, 3243–3250.
(12) Veal, J. M.; Rill, R. L. *Biochemistry* **1991**, *30*, 1132–1140.
(13) Gorner, H.; Tossi, A. B.; Stradowski, C.; Schulte-Frohlinde, D. *J. Photochem. Photobiol. B* **1988**, *2*, 67–89.
(14) Benites, P. J.; Holmberg, R. C.; Rawat, D. S.; Kraft, B. J.; Klein, L. J.; Peters, D. G.; Thorp, H. H.; Zaleski, J. M. *J. Am. Chem. Soc*. **2003**, *125*, 6434–6446.
(15) Zeglis, B. M.; Boland, J. A.; Barton, J. K. *J. Am. Chem. Soc*. **2008**, *130*, 7530–7531.

and $[Rh(bpy)_2(phzi)]^{3+}$ preferentially bind to sites of weaker base pair interactions such as mismatches or abasic sites.[7,15−19] For example, the DNA-binding affinity of $[\Delta\text{-}Rh(bpy)_2(chrysi)]^{3+}$ is 1000-fold greater for mismatched sites than for normal DNA base pairs.[15,17,19] Analogously, $[Ru(phen)_2dppz]^{2+}$ preferentially undergoes metallo-insertion instead of intercalative binding upon encountering DNA mismatches and abasic sites.[20] Additionally, sequence specific binding can be achieved by designing ancillary ligand targeting that maximize intermolecular interactions such as H-bonding and van der Waals contacts with the DNA sequence of interest.[21,22]

The ability to confidently rely on luminescent probes for DNA structural interrogation has only come through extensive characterization of the DNA binding modes and binding specificity of these types of transition metal complexes using X-ray crystallography, NMR spectroscopy, DNA footprinting and cleavage gel assays, and competitive binding displacement assays.[7,15−17,19,20,23−36] Metal-based probes typically exhibit strong, MLCT-based molecular light switch emission, where a large increase in luminescence quantum yield is detectable upon DNA binding. The most widely studied light switch compound, $[Ru(phen)_2dppz]^{2+}$, displays a 10^4-fold increase in luminescence intensity when bound to DNA in aqueous solution.[9]

Extensive photophysical studies have shown that the unusual binary luminescent behavior of $[Ru(phen)_2dppz]^{2+}$ in the presence and absence of DNA is the result of two interacting ^{3}MLCT excited states, a highly emissive "light" state where the charge-transfer generated negative charge is localized on the phenanthroline components of the ligands ($^3MLCT_{phen}$), as well as a second, much more weakly emissive "dark" state where the negative charge is localized on the phenazine portion of the dppz ligand ($^3MLCT_{phzn}$).[9,30,34,37−49] The lower energy $^3MLCT_{phzn}$ is stabilized and deactivated in the presence of solvents that can H-bond to the periphery phenazine nitrogens resulting in quenching of the emissive $^3MLCT_{phen}$ state. DNA intercalation of the dppz ligand leads to an increase in solvent shielding of the phenazine nitrogens, which reduces the non-radiative decay rate and increases the emissive quantum yield of the complex. Since $[Ru(phen)_2dppz]^{2+}$ has a very short lifetime ($\tau \sim 3$ ps) and marginal emission quantum yield ($\phi \sim 10^{-7}$) in aqueous solution, the turn-on effect is significant.[45] However, even DNA solvent shielding does not result in an extensive lifetime ($\tau_{DNA} \sim 75, 250$ ns) or an impressively high emission quantum yield ($\phi_{DNA} \sim 0.02$) as is typical of commercial dye-based diagnostics.[9]

One possible approach for enhancing the emissive lifetime and quantum yield is to perturb the excited state dynamics by mixing a low-lying $^3\pi\pi^*$ ligand-based state with the emissive ^{3}MLCT state.[50] Since these ligand states typically have much longer lifetimes, the luminescence characteristics of the complex can be tuned depending upon the thermodynamics of the ^{3}MLCT manifold and the intervening $^3\pi\pi^*$ state. Within this theme, the excited state dynamics of some Re(I) dppz complexes do indeed exhibit perturbed kinetics because of rapid interconversion between the emissive ^{3}MLCT and the ligand-localized $^3\pi\pi^*$ state.[51,52] In contrast to Ru(II)-dppz complexes where the $^3\pi\pi^*$ ligand-based state lies to higher energy than the ^{3}MLCT manifold and plays no role in the observed photophysics,[38] perturbations to the classic ^{3}MLCT luminescence from the $^3\pi\pi^*$ state are observed in *fac*-$[Re(CO)_3(dppz)L]$ complexes.[51,52] The relative populations of the three states and the rate of interconversion between them are dependent on the structure and environment of the complex.

---

(16) Zeglis, B. M.; Boland, J. A.; Barton, J. K. *Biochemistry* **2009**, *48*, 839–849.

(17) Zeglis, B. M.; Pierre, V. C.; Kaiser, J. T.; Barton, J. K. *Biochemistry* **2009**, *48*, 4247–4253.

(18) Junicke, H.; Hart, J. R.; Kisko, J.; Glebov, O.; Kirsch, I. R.; Barton, J. K. *Proc. Natl. Acad. Sci. U. S. A.* **2003**, *100*, 3737–3742.

(19) Zeglis, B. M.; Barton, J. K. *Nat. Protoc.* **2007**, *2*, 357–371.

(20) Lim, M. H.; Song, H.; Olmon, E. D.; Dervan, E. E.; Barton, J. K. *Inorg. Chem.* **2009**, *48*, 5392–5397.

(21) Sitlani, A.; Barton, J. K. *Biochemistry* **1994**, *33*, 12100–12108.

(22) Sitlani, A.; Dupureur, C. M.; Barton, J. K. *J. Am. Chem. Soc.* **1993**, *115*, 12589–12590.

(23) Kielkopf, C. L.; Erkkila, K. E.; Hudson, B. P.; Barton, J. K.; Rees, D. C. *Nat. Struct. Biol.* **2000**, *7*, 117–121.

(24) Pierre, V. C.; Kaiser, J. T.; Barton, J. K. *Proc. Natl. Acad. Sci. U. S. A.* **2007**, *104*, 429–434.

(25) Hudson, B. P.; Barton, J. K. *J. Am. Chem. Soc.* **1998**, *120*, 6877–6888.

(26) Hudson, B. P.; Dupureur, C. M.; Barton, J. K. *J. Am. Chem. Soc.* **1995**, *117*, 9379–9380.

(27) Rueba, E.; Hart, J. R.; Barton, J. K. *Inorg. Chem.* **2004**, *43*, 4570–4578.

(28) Zhen, Q. X.; Ye, B. H.; Liu, J. G.; Zhang, Q. L.; Ji, L. N.; Wang, L. *Inorg. Chim. Acta* **2000**, *303*, 141–147.

(29) Zhen, Q. X.; Ye, B. H.; Zhang, Q. L.; Liu, J. G.; Li, H.; Ji, L. N.; Wang, L. *J. Inorg. Biochem.* **1999**, *76*, 47–53.

(30) Chen, W.; Turro, C.; Friedman, L. A.; Barton, J. K.; Turro, N. J. *J. Phys. Chem. B* **1997**, *101*, 6995–7000.

(31) Coates, C. G.; Callaghan, P.; McGarvey, J. J.; Kelly, J. M.; Jacquet, L.; Kirsch-De Mesmaeker, A. *J. Mol. Struct.* **2001**, *598*, 15–25.

(32) Delaney, S.; Pascaly, M.; Bhattacharya, P. K.; Han, K.; Barton, J. K. *Inorg. Chem.* **2002**, *41*, 1966–1974.

(33) Hiort, C.; Lincoln, P.; Norden, B. *J. Am. Chem. Soc.* **1993**, *115*, 3448–3454.

(34) Holmlin, R. E.; Stemp, E. D. A.; Barton, J. K. *Inorg. Chem.* **1998**, *37*, 29–34.

(35) Yam, V. W.-W. V.; Lo, K. K.-W.; Cheung, K.-K.; Kong, R. Y.-C. *J. Chem. Soc., Dalton Trans.* **1997**, 2067–2072.

(36) Zhang, Q.-L.; Liu, J.-H.; Liu, J.-Z.; Zhang, P.-X.; Ren, X.-Z.; Liu, Y.; Huang, Y.; Ji, L.-N. *J. Inorg. Biochem.* **2004**, *98*, 1405–1412.

(37) Brennaman, M. K.; Alstrum-Acevedo, J. H.; Fleming, C. N.; Jang, P.; Meyer, T. J.; Papanikolas, J. M. *J. Am. Chem. Soc.* **2002**, *124*, 15094–15098.

(38) Brennaman, M. K.; Meyer, T. J.; Papanikolas, J. M. *J. Phys. Chem. A* **2004**, *108*, 9938–9944.

(39) Coates, C. G.; Callaghan, P. L.; McGarvey, J. J.; Kelly, J. M.; Kruger, P. E.; Higgins, M. E. *J. Raman Spectrosc.* **2000**, *31*, 283–288.

(40) Coates, C. G.; McGarvey, J. J.; Callaghan, P. L.; Coletti, M.; Hamilton, J. G. *J. Phys. Chem. B* **2001**, *105*, 730–735.

(41) Coates, C. G.; Olofsson, J.; Coletti, M.; McGarvey, J. J.; Oenfelt, B.; Lincoln, P.; Norden, B.; Tuite, E.; Matousek, P.; Parker, A. W. *J. Phys. Chem. B* **2001**, *105*, 12653–12664.

(42) Nair, R. B.; Cullum, B. M.; Murphy, C. J. *Inorg. Chem.* **1997**, *36*, 962–965.

(43) Nair, R. B.; Murphy, C. J. *J. Inorg. Biochem.* **1998**, *69*, 129–133.

(44) Olofsson, J.; Onfelt, B.; Lincoln, P.; Norden, B.; Matousek, P.; Parker, A. W.; Tuite, E. *J. Inorg. Biochem.* **2002**, *91*, 286–297.

(45) Olson, E. J. C.; Hu, D.; Hoermann, A.; Jonkman, A. M.; Arkin, M. R.; Stemp, E. D. A.; Barton, J. K.; Barbara, P. F. *J. Am. Chem. Soc.* **1997**, *119*, 11458–11467.

(46) Onfelt, B.; Lincoln, P.; Norden, B.; Baskin, J. S.; Zewail, A. H. *Proc. Natl. Acad. Sci. U. S. A.* **2000**, *97*, 5708–5713.

(47) Fees, J.; Kaim, W.; Moscherosch, M.; Matheis, W.; Klima, J.; Krejcik, M.; Zalis, S. *Inorg. Chem.* **1993**, *32*, 166–174.

(48) Browne, W. R.; McGarvey, J. J. *Coord. Chem. Rev.* **2006**, *250*, 1696–1709.

(49) McGarvey, J. J.; Callaghan, P.; Coates, C. G.; Schoonover, J. R.; Kelly, J. M.; Jacquet, L.; Gordon, K. C. *J. Phys. Chem. B* **1998**, *102*, 5941–5942.

(50) Wang, X.-Y.; Del Guerzo, A.; Schmehl, R. H. *J. Photochem. Photobiol., C* **2004**, *5*, 55–77.

(51) Kuimova, M. K.; Alsindi, W. Z.; Blake, A. J.; Davies, E. S.; Lampus, D. J.; Matousek, P.; McMaster, J.; Parker, A. W.; Towrie, M.; Sun, X.-Z.; Wilson, C.; George, M. W. *Inorg. Chem.* **2008**, *47*, 9857–9869.

(52) Schoonover, J. R.; Bates, W. D.; Meyer, T. J. *Inorg. Chem.* **1995**, *34*, 6421–6422.

As expected for these environment-sensitive molecules, the observed photophysics are variable upon ligand substitution, substituent modification of the dppz ligand, changes in solvent dielectric constant, or changes in temperature.[51,52]

Our interests in metal complex photophysics stem from the ability to employ extended π-conjugation[53-55] or metal-ligand charge transfer excitation to promote ligand-based diradical generation for nuclease applications.[14,56-58] In related work, we have developed the enediyne-chelated complex, $[Cu(bpod)_2]^{2+}$ (bpod = *cis*-1,8-bis(pyridin-3-oxy)oct-4-ene-2,6-diyne), that can intercalate DNA and upon photoexcitation, performs DNA strand scission by C-4′ H-atom abstraction.[14] Unfortunately, DNA binding of this complex and related structures has been difficult to characterize since their spectroscopic signatures are only very modestly perturbed by interactions with DNA. The desire for compounds that act as self-reporters for DNA binding led us to develop enediyne analogues of $[Ru(phen)_2dppz]^{2+}$ based on the alkynylated ligands 2,3-bis(phenylethynyl)-1,4,8,9-tetraaza-triphenylene (bptt, **1**) and 2,3-bis(4-*tert*-butyl-phenylethynyl)-1,4,8,9-tetraaza-triphenylene (tbptt, **2**). $[Ru(phen)_2(bptt)]^{2+}$ exhibits molecular light switch behavior upon binding to DNA while the sterically hindered $[Ru(phen)_2(tbptt)]^{2+}$ complex is unable to intercalate into the DNA helix. More subtly, the extended π-conjugation of **1** relative to dppz lowers the energy of the $^3\pi\pi^*$ excited state leading to participation of this state in the observed photophysical behavior, similar to that for Re(I) dppz complexes and unlike that for $[Ru(phen)_2dppz]^{2+}$.

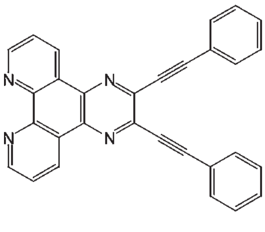

1

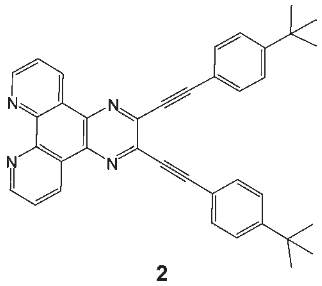

2

Experimental Section

Materials. All air sensitive manipulations were performed under nitrogen using Schlenk and drybox techniques. Tetrahydrofuran was dried by distillation over sodium/benzophenone. All chemicals used in the syntheses and characterizations were of the highest purity available from Aldrich and Fluka and were used as received. $Ru(phen)_2Cl_2$[59] and 5,6-diamino-1,10-phenanthroline[60,61] were prepared according to literature methods. The dione, 1,6-bisphenyl-hexa-1,5-diyne-3,4-dione,[62] and bptt[63,64] were synthesized using modified literature procedures.

Physical Measurements. Samples were prepared using volumetric glassware, and standard Schlenk and drybox techniques. Solvents were degassed by either purging with N_2 for > 1 h, or several freeze-pump thaw cycles. ^1H NMR spectra were collected on a Varian Inova 400 NMR spectrometer with the proton-solvent as a reference. Elemental analyses were performed by Atlantic Microanalytical Laboratory, Norcross, GA. Electronic absorption spectra were collected on a Perkin-Elmer Lambda 19 UV/Vis/NIR spectrometer at ambient temperature. Luminescence measurements were obtained with a Perkin-Elmer LS 50B luminescence spectrometer equipped with a Hamatatsu model R928 PMT. Quantum yields are given for solutions of matched optical density at the excitation wavelength, and are reported relative to the fluorescence of quinine sulfate in 1 N H_2SO_4 (ϕ = 0.55, λ_{ex} = 345 nm),[65] for the high energy ligand fluorescence, and $[Ru(bpy)_3]Cl_2$ in air-equilibrated water (ϕ = 0.028 λ_{ex} = 465 nm)[66] for luminescence of metal complexes. Quantum yields have an experimental error of ±5%. Solid-state low temperature emission measurements were collected with the sample submerged in liquid nitrogen using a finger dewar. Solution temperatures above ambient were achieved by immersion in a warm water bath. Solution temperatures below room temperature were achieved by immersion in an ice bath or liquid nitrogen slurries of acetonitrile or acetone and are accurate to within ±2 °C. The triplet-sensitized luminescence spectrum of **1** was obtained by exciting a 50 μM solution of **1** with 100 μM xanthone (Aldrich) at λ_{ex} = 355 nm.

Samples containing DNA were prepared via dilution of a stock solution of calf thymus DNA (Sigma) in a buffer of 10 mM Tris-HCl (pH = 7.8) which gave an A_{260}:A_{280} ratio of 1.9:1, indicating that the DNA was sufficiently free of protein.[67] DNA concentrations are expressed as the concentration of bases, which was determined by measurements of the optical density at 260 nm (ε = 6,600 M^{-1} cm^{-1} per base).[68] For the DNA binding affinity determination, the luminescence spectra of a 50 μM solution of **3** in 10 mM Tris-HCl (pH = 7.8) containing 200 mM NaCl and 10 mM $MgCl_2$ were recorded as a function of increasing CT-DNA concentration (λ_{ex} = 399 nm) with a Perkin-Elmer LS 50B luminescence spectrometer. A binding isotherm was constructed using the average luminescence intensity at 600 nm for three trials and was fit using the Kaleidagraph software package to a one site binding model on a per base pair basis. The observed luminescence intensity is the sum of the luminescence from the free and bound states and can be defined as $I = I_f + \theta I_b$, where I is the measured luminescence intensity, I_f, and I_b are the luminescence intensity of the free and bound forms of **3**, and θ is the fraction of **3** bound. The fraction bound is equal to $R \cdot D/R_t$, where $R \cdot D$ is the concentration of **3** bound to DNA and R_t is the total concentration of **3**. In the equilibrium expression for K_d, the dissociation constant is expressed in terms of R_t and D_t, where D_t is the total concentration of DNA bp, since those are known quantities and $R \cdot D$ is not directly measured. The value of θ is then obtained directly from these parameters (eq 1).

$$I = I_f + I_b \frac{(R_t + D_t + K_d) - \sqrt{(R_t + D_t + K_d)^2 - 4R_tD_t}}{2D_t} \qquad (1)$$

Because the experimental concentrations are on the order of K_d, no additional assumption could be made to simplify the expression. I_f,

---

(53) Chandra, T.; Kraft, B. J.; Huffman, J. C.; Zaleski, J. M. *Inorg. Chem.* **2003**, *42*, 5158–5172.

(54) Nath, M.; Pink, M.; Zaleski, J. M. *J. Am. Chem. Soc.* **2005**, *127*, 478–479.

(55) Koepke, T.; Pink, M.; Zaleski, J. M. *Org. Biomol. Chem.* **2006**, *4*, 4059–4062.

(56) Kraft, B. J.; Eppley, H. J.; Huffman, J. C.; Zaleski, J. M. *J. Am. Chem. Soc.* **2002**, *124*, 272–280.

(57) Kraft, B. J.; Zaleski, J. M. *New J. Chem.* **2001**, *25*, 1281–1289.

(58) Maurer, T. D.; Kraft, B. J.; Lato, S. M.; Zaleski, J. M.; Ellington, A. D. *Chem. Commun.* **2000**, 69–70.

(59) Sullivan, B. P.; Salmon, D. J.; Meyer, T. J. *Inorg. Chem.* **1978**, *17*, 3334–3341.

(60) Bodige, S.; MacDonnell, F. M. *Tetrahedron Lett.* **1997**, *38*, 8159–8160.

(61) Yamada, M.; Tanaka, Y.; Yoshimoto, Y.; Kuroda, S.; Shimao, I. *Bull. Chem. Soc. Jpn.* **1992**, *65*, 1006–1011.

(62) Faust, R.; Weber, C.; Fiandanese, V.; Marchese, G.; Punzi, A. *Tetrahedron* **1997**, *53*, 14655–14670.

(63) Choy, N.; Russell, K. C. *Heterocycles* **1999**, *51*, 13–16.

(64) Faust, R.; Ott, S. *J. Chem. Soc., Dalton Trans.* **2002**, 1946–1953.

(65) Guilbault, G. G. *Practical Fluorescence*, 2nd ed.; M. Dekker: New York, 1990; p 812.

(66) Nakamaru, K. *Bull. Chem. Soc. Jpn.* **1982**, *55*, 2697–2705.

(67) Marmur, J. *J. Mol. Biol.* **1961**, *3*, 208–218.

(68) Reichmann, M. E.; Rice, S. A.; Thomas, C. A.; Dotty, P. *J. Am. Chem. Soc.* **1954**, *76*, 3047–3053.

I_b, and K_d were determined from the fit, and the binding association constant obtained by taking the reciprocal of the K_d.

Time-resolved luminescence and absorption measurements were performed using the third harmonic of a Coherent Infinity 40−100 pulsed Nd:YAG laser operating at a repetition rate of 10 Hz, (fwhm =5 ns). The laser ouput was used to pump a Lambda Physik Scanmate OPPO (λ = 450 nm) or was Raman-shifted (λ = 396.0 or 447.7 nm) using 500 psi methane gas contained with a cylindrical chamber 1 m in length and 0.06 m in diameter. The laser beam was focused in the center of the chamber, and a Pellin-Broca prism was used to separate and select the desired output wavelength. For transient absorption measurements, the probe beam originated from a PTI model LPS-220 water cooled 150 W Xe arc lamp that was chopped at a rate of 10 Hz (fwhm ~15 ms). The pump and probe beams converged on a 2 mm quartz cell at a ≈ 10° angle. The probe beam was then focused onto the entrance slit of an ISA model 340S single monochromator equipped with two gratings (1200 grooves/mm and 600 grooves/mm) and two output ports. Kinetics measurements were made utilizing the 1200 groove/mm (500 nm blaze) grating and a Hamamatsu R928P photomultiplier tube. The output from the photomultiplier was fed through a variable gain, broadband amplifier and recorded on a Tektronix (TDS 380) digital oscilloscope. For emission kinetics measurements, a 90° sampling arrangement was utilized where the diffuse emission was focused into the single monochromator. Spectral measurements were performed utilizing the 600 groove/mm (500 nm blaze) grating and a gated ICCD (Princeton Instruments) with a 24.8 mm × 6.2 mm active area (1024 × 256 pixel array). All reported lifetimes have an error of ±5%.

Solid-state Raman spectra were collected with a Renishaw 1000B micro-Raman spectrometer operating with a λ = 785 nm SDL diode laser. Resonance Raman spectra were collected using Ar^+ (λ = 457.9, 488.0, and 501.7 nm) and Kr^+ (λ = 406.7 nm) ion lasers (Coherent models I-70 and I-300, respectively) operating at 100 mW (50 mW at sample). Plasma lines were removed using 600 (λ = 457.9, 488.0, and 501.7 nm) or 1200 grooves/mm (λ = 406.7 nm) gratings prior to the sample. The backscattering was collected with a Nikkor 85 mm 1:1.4 lens focused through a depolarizer (CVI) onto a custom-built f/4 subtractive double monochromator equipped with 600 groove/mm gratings (500 nm blaze). The output from the double monochromator was focused onto the entrance slit of an Action Spectropro 500i monochromator (f/6.5) operating with a 1800 groove/mm (500 nm blaze) for spectra collected using λ = 457.9, 488.0, and 501.7 nm and a 2400 groove/mm (400 nm blaze) for spectra collected utilizing λ = 406.7 nm excitation. The disperse scattering was then focused onto a back-illuminated LN_2 cooled CCD (Princeton Instruments) with a 30 mm ×14.4 mm active area (2500 × 600 pixel array).

Synthesis of 1,6-Bisphenyl-hexa-1,5-diyne-3,4-dione.[62] A 2.85 mL portion of *n*-butyllithium (1.6 M in hexanes) was added to a stirring solution of 0.50 mL (4.55 mmol) of phenylacetylene in 5 mL of tetrahydrofuran at −78 °C, and the resulting mixture was stirred for 30 min at −78 °C. This solution was added to a mixture of 653 mg (4.55 mmol) of CuBr and 790 mg (9.10 mmol) of LiBr dissolved in 30 mL of tetrahydrofuran at 0 °C. To this reaction mixture, 5.75 mL (2.27 mmol) of oxalyl chloride in 30 mL of tetrahydrofuran was added dropwise. The solution was stirred for 1 h at 0 °C and subsequently quenched with 100 mL of saturated aqueous NH_4Cl. The crude product was extracted with ethyl acetate (3 × 100 mL) and dried over Na_2SO_4. The solution was then filtered and concentrated under vacuum. The crude product was purified by flash chromatography (4:1 hexanes:ethyl acetate). Yield: 455 mg (78%). ^{1}H NMR (CD_3OD, δ ppm): 7.31 (d, 2H); 7.41 (d, 4H); 7.58 (dd, 4H). ^{13}C NMR (CD_3OD, δ ppm): 86.0, 99.9, 118.9, 128.5, 131.6, 133.7, 172.3.

Synthesis of 1,6-Bis-(4-*tert*-butyl-phenyl)-hexa-1,5-diyne-3,4-dione. This compound was prepared in a manner identical to 1,6-bisphenyl-hexa-1,5-diyne-3,4-dione. The crude product was purified by flash chromatography (10:1 hexanes:ethyl acetate) to give a bright yellow solid in 66% yield. ^{1}H NMR ($CDCl_3$, δ ppm): 7.65 (d, 4H); 7.46 (d, 4H); 1.35 (s, 18H). ^{13}C ($CDCl_3$, δ ppm): 31.0, 35.2, 86.2, 100.8, 116.1, 125.9, 133.9, 155.9, 172.7. HRMS (EI): Calcd for $C_{26}H_{26}O_2$ 370.4834. Found 370.4845 (M^+).

Synthesis of 2,3-Bis(phenylethynyl)-1,4,8,9-tetraaza-triphenylene (bptt, 1).[63,64] A sample of 0.061 g (0.29 mmol) of 1,6-bisphenyl-hexa-1,5-diyne-3,4-dione and 0.075 g (0.29 mmol) 5,6-diamino-1,10-phenanthroline were dissolved in 3 mL of glacial acetic acid. The resulting solution was stirred for 5 min and then filtered. The pale yellow solid was washed with 2 mL of acetic acid then 5 mL of methanol and dried under vacuum. Yield: 123 mg (98%). Mp: 292 °C. ^{1}H NMR (CD_2Cl_2, δ ppm): 7.48 (m, 6H); 7.76 (m, 4H); 7.82 (dd, 2H); 9.24 (dd, 2H); 9.49 (dd, 2H). ^{13}C NMR (CD_2Cl_2, δ ppm): 86.7, 96.9, 122.1, 124.2, 126.2, 129.1, 130.2, 132.6, 133.6, 138.2, 141.9, 148.1, 152.8. MS (EI): *m*/*z* 432.1 (M^+). Anal. Calcd for $C_{30}H_{16}N_4$: C, 83.32; H, 3.73; N, 12.95. Found: C, 83.21; H, 3.82; N, 12.76.

Synthesis of 2,3-Bis(4-*tert*-butyl-phenylethynyl)-1,4,8,9-tetraaza-triphenylene (tbptt, 2). 5,6-Diamino-1,10-phenanthroline (0.127 g, 0.604 mmol) and 1,6-bis-(4-*tert*-butyl-phenyl)-hexa-1,5-diyne-3,4-dione (0.228 g, 0.616 mmol) were dissolved in 5 mL of glacial acetic acid. The resulting solution was stirred for 5 min and then filtered. The bright yellow solid was washed with acetic acid, then methanol, and dried under vacuum. Yield: 250 mg (76%). ^{1}H NMR ($CDCl_3$, δ ppm): 9.40 (dd, 2H); 9.20 (d, 2H); 7.77 (dd, 2H); 7.67 (d, 4H); 7.48 (d, 4H); 1.32 (s, 18H). ^{13}C NMR ($CDCl_3$, δ ppm): 31.2, 35.3, 86.7, 97.3, 118.8, 124.4, 126.2, 126.7, 132.4, 133.6, 138.3, 141.4, 147.9, 152.6, 154.0. HRMS (EI): Calcd for $C_{38}H_{32}N_4$ 544.26270. Found 544.26273 (M^+).

Synthesis of [Ru(phen)$_2$bptt](PF$_6$)$_2$ (3). To a stirring solution of 0.185 g (0.347 mmol) of $Ru(phen)_2Cl_2$ in 20 mL of methanol, 0.150 g (0.347 mmol) of **1** and 0.131 g (0.764 mmol) of $NaCF_3SO_3$ were added, and the reaction mixture was allowed to reflux for 2 h. The NaCl precipitate was filtered, and 25 mL of saturated aqueous NH_4PF_6 was added to the filtrate to precipitate the product. The solution was filtered, and the solid was dried under vacuum and recrystallized from methanol. Yield: 150 mg (37%). X-ray quality crystals were grown from a saturated CH_2Cl_2 solution layered with ethanol. ^{1}H NMR (DMSO, δ ppm): 9.38 (d, 2H); 8.79 (d, 2H); 8.77 (d, 2H); 8.40 (s, 4H); 8.23 (dd, 4H); 8.06 (d, 2H); 7.86−7.73 (m, 10H); 7.58−7.52 (m, 6H). ^{13}C NMR (DMSO, δ ppm): 86.4, 97.7, 120.1, 126.3, 126.4, 127.5, 128.1, 128.5, 129.3, 130.5, 130.9, 132.1, 133.2, 137.0, 137.6, 141.1, 147.1, 149.7, 152.7, 153.3, 154.4. MS (ESI): *m*/*z* 1039.4 $[M - PF_6]^+$. Anal. Calcd for $C_{54}H_{32}N_8P_2F_{12}Ru$: C, 54.78; H, 2.72; N, 9.46. Found: C, 54.52; H, 2.82; N, 9.22.

Synthesis of [Ru(phen)$_2$tbptt](PF$_6$)$_2$ (4). Complex **4** was prepared utilizing a modified literature procedure.[64] To a degassed mixture of 20 mL of ethanol, 5 mL of dichloromethane, and 0.115 g (0.211 mmol) of **2**, 113 mg (0.200 mmol) of $Ru(phen)_2Cl_2$ was added. The resulting solution was heated to 100 °C and allowed to stir for 18 h under nitrogen. The mixture was then cooled to 0 °C, and 3 mL of a saturated aqueous solution of NH_4PF_6 was added to generate a red-orange precipitate. The solution was filtered, and the precipitate washed with water, ethanol, and ether, then recrystallized from methanol to give **4**. Yield: 205 mg (79%). ^{1}H NMR (DMSO, δ ppm): 9.39 (d, 2H); 8.79 (d, 2H); 8.77 (d, 2H); 8.40 (s, 4H); 8.25 (d, 2H); 8.21 (d, 2H); 8.06 (d, 2H); 7.82 (m, 6H); 7.68 (d, 4H); 7.55 (d, 4H); 1.31 (s, 18H). ^{13}C NMR (DMSO, δ ppm): 30.8, 34.9, 86.1, 98.0, 117.3, 126.1, 127.4, 128.1, 128.5, 130.5, 132.0, 137.0, 137.3, 141.2, 147.1, 149.6, 152.7, 153.4, 153.8, 154.3. MS (ESI): *m*/*z* 1151.1 $[M - PF_6]^+$. Anal. Calcd for $C_{62}H_{48}F_{12}N_8P_2Ru$: C, 57.45; H, 3.73; N, 8.65; Found: C, 57.52; H, 3.72; N, 8.52.

Crystallographic Structure Determination of 3. An orange crystal of **3** (approximate dimensions 0.08 × 0.005 × 0.003 mm^3) was placed onto the tip of a 0.001 mm diameter glass capillary and mounted on a Kappa SMART setup equipped with a 2 × 2 array of 1K CCD detectors at beamline 15ID, ChemMatCARS, APS

Chicago, for a data collection at 123(2) K. The data collection was carried out using λ = 0.56356 Å (energy: 22.113 keV, monochromator: two diamond 1 1 1 crystals, using two mirrors to exclude higher harmonics) with a frame time of 5 s and a detector distance of 6 cm. Frames were collected with 0.30° steps in ϕ and at 0° for all other angles. The data reduction was carried out with SAINT[69] using the orientation matrix of the major twin component and including data to a resolution of 0.8238 Å (40° for silver radiation). The space group $P\bar{1}$ was determined based on intensity statistics and the lack of systematic absences. A direct-methods solution was calculated which provided most non-hydrogen atoms from the E-map.[70] Full-matrix least-squares/difference Fourier cycles were performed which located the remaining non-hydrogen atoms.[71] All non-hydrogen atoms of the Ru-complex were refined with anisotropic displacement parameters. The data were corrected for non-merohedral twinning[72] (twin law by rows −1 0 0, 0.291 1 −1.028, 0 0 −1) in the final refinements, which resulted in significantly decreased *R*-values and a clean difference map. The structure was found with two independent molecules in the asymmetric unit, related by pseudo-symmetry. The two independent molecules were restrained to be geometrically the same within 0.001 Å. The packing plot shows that the ruthenium complexes π-stack along the *a*-axis with distances between the pyrazine rings of 3.51 Å between the independent molecules and 3.83 and 3.75 Å between molecule A and its symmetry equivalent and molecule B and its symmetry equivalent, respectively.

Computational Methods and Vibrational Analysis. Geometry optimizations for **1** and **3** were performed using density functional theory (DFT) and the B3LYP combination of functionals available in Gaussian 98.[73−75] A 6-31G* basis set was used for all calculations involving **1**. For **3**, the LANLDZ effective core potential was used for Ru^{2+} and a 3-21G basis set was used for the C, N, and H atoms.[76−78] Since the crystal structure of **3** was not an energetic minimum in the gas phase, only the vibrational analysis at the gas phase B3LYP optimized geometry of **3** is presented here. The DFT vibrational frequencies were scaled by 0.9497 resulting in values that were in good agreement with the experimental results for known vibrations such as −C≡C−. For **1**, time-dependent DFT (TDDFT) calculations were performed with the same functionals and basis set at the optimized geometry to obtain electronic transition energies.

Results and Discussion

Synthesis. The dione precursors to **1** and **2** were obtained utilizing a modified literature procedure.[62] Slow addition of the appropriate lithium-phenylacetylene salt to a CuBr solution followed by the addition of oxalyl chloride results in yields of ∼65−80% of the dione precursors. The subsequent condensation reaction of the dione with 5,6-diamino-1,10-phenanthroline[63,64] afforded ligands **1** and **2** in 98% and 76% yield, respectively. The complexation reactions were performed via addition of the ligand to a solution of Ru(phen)$_2$Cl$_2$. The higher yield of **4** primarily derives from the use of solvent conditions suitable for complete dissolution of **2** (4:1 EtOH:CH$_2$Cl$_2$) and longer reaction times (18 h).

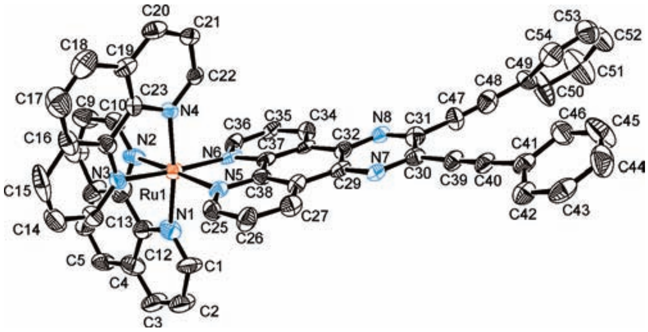

Figure 1. ORTEP of the X-ray crystal structure of **3**. Thermal ellipsoids are illustrated at 30% probability.

X-ray Crystal Structure of 3. Crystals suitable for X-ray structure determination were obtained by layering and slow diffusion of ethanol into a saturated dichloromethane solution of **3**. Crystals of **3** were small and required evaluation using the synchrotron source at Argonne National Laboratory. The crystal was twinned and poorly diffracting leading to a lower quality structure, but it was sufficient for the purposes of the present discussion. The crystallographic data for **3** are presented in the Supporting Information, Table S1. An ORTEP illustration of the crystal structure is shown in Figure 1. The Ru(II)-center possesses a distorted octahedral coordination sphere as a consequence of the small bite angles (average = 79.2°) of the bidentate ligands. The mean Ru−N bond length (2.08 Å) falls within the range typical for [Ru(diimine)$_3$]$^{2+}$ complexes.[79−86] It is slightly longer than those reported for [Ru(phen)$_3$](PF$_6$)$_2$ (2.07 Å)[81] and [Ru(bpy)$_3$](PF$_6$)$_2$ (2.056 Å)[79] but shorter than those reported for [Ru(Me$_2$phen)$_2$dppz](PF$_6$)$_2$ (2.10 Å).[83] The C31−C47−C48 (175.4° (13)) and C30−C39−C40 (173.9° (11)) bond angles of the enediyne unit do not significantly deviate from linearity. The distance between the alkyne termini (4.17 Å) is large, but typical for stable acyclic enediyne motifs.[87,88] The

---

[69] Glazer, E. C.; Magde, D.; Tor, Y. *J. Am. Chem. Soc.* **2007**, *129*, 8544–8551.

[70] Altomare, A.; Cascarano, G.; Giacovazzo, C.; Guagliardi, A.; Burla, M. C.; Polidori, G.; Camalli, M. *J. Appl. Crystallogr.* **1994**, *27*, 435.

[71] Sheldrick, G. *Acta Crystallogr., Sect. A* **2008**, *64*, 112–122.

[72] Young, V. *ROTWIN, Program for data correction for non-merohedral twins*; unpublished.

[73] Frisch, M. J.; Trucks, G. W.; Schlegel, H. B.; Scuseria, G. E.; Robb, M. A.; Cheeseman, J. R.; Zakrzewski, V. G.; Montgomery, J. A. J.; Stratmann, R. E.; Burant, J. C.; Dapprich, S.; Millam, J. M.; Daniels, A. D.; Kudin, K. N.; Strain, M. C.; Farkas, O.; Tomasi, J.; Barone, V.; Cossi, M.; Cammi, R.; Mennucci, B.; Pomelli, C.; Adamo, C.; Clifford, S.; Ochterski, J.; Petersson, G. A.; Ayala, P. Y.; Cui, Q.; Morokuma, K.; Malick, D. K.; Rabuck, A. D.; Raghavachari, K.; Foresman, J. B.; Cioslowski, J.; Ortiz, J. V.; Baboul, A. G.; Stefanov, B. B.; Liu, G.; Laishenko, A.; Piskorz, P.; Komaromi, I.; Gomperts, R.; Martin, R. L.; Fox, D. J.; Keith, T.; Al-Laham, M. A.; Peng, C. Y.; Nanayakkara, A.; Gonzalez, C.; Callacombe, M.; Gill, P. M. W.; Head-Gordon, M.; Replogle, E. S.; Pople, J. A. *Gaussian 98*, Revision A.6; Gaussian,Inc.: Pittsburgh, PA, **1998**.

[74] Lee, C.; Yang, W.; Parr, R. G. *Phys. Rev. B: Condens. Matter* **1988**, *37*, 785–789.

[75] Becke, A. D. *J. Chem. Phys.* **1993**, *98*, 5648–5652.

[76] Hay, P. J.; Wadt, W. R. *J. Chem. Phys.* **1985**, *82*, 270–283.

[77] Hay, P. J.; Wadt, W. R. *J. Chem. Phys.* **1985**, *82*, 299–310.

[78] Wadt, W. R.; Hay, P. J. *J. Chem. Phys.* **1985**, *82*, 284–298.

[79] Rillema, D. P.; Jones, D. S.; Levy, H. A. *Chem. Commun.* **1979**, 849–851.

[80] Rutherford, T. J.; Pellegrini, P. A.; Aldrich-Wright, J.; Junk, P. C.; Keene, F. R. *Eur. J. Inorg. Chem.* **1998**, 1677–1688.

[81] Maloney, D. J.; MacDonnell, F. M. *Acta Crystallogr., Sect. C* **1997**, *C53*, 705–707.

[82] Komatsuzaki, N.; Katoh, R.; Himeda, Y.; Sugihara, H.; Arakawa, H.; Kasuga, K. *J. Chem. Soc., Dalton Trans.* **2000**, 3053–3054.

[83] Liu, J.-G.; Zhang, Q.-L.; Shi, X.-F.; Ji, L.-N. *Inorg. Chem.* **2001**, *40*, 5045–5050.

[84] Greguric, A.; Greguric, I. D.; Hambley, T. W.; Aldrich-Wright, J. R.; Collins, J. G. *J. Chem. Soc., Dalton Trans.* **2002**, 849–855.

[85] Berg-Brennan, C.; Subramanian, P.; Absi, M.; Stern, C.; Hupp, J. T. *Inorg. Chem.* **1996**, *35*, 3719–3722.

[86] Breu, J.; Stoll, A. J. *Acta Crystallogr., Sect. C* **1996**, *C52*, 1174–1177.

[87] Rawat, D. S.; Benites, P. J.; Incarvito, C. D.; Rheingold, A. L.; Zaleski, J. M. *Inorg. Chem.* **2001**, *40*, 1846–1857.

[88] Kraft, B. J.; Coalter, N. L.; Nath, M.; Clark, A. E.; Siedle, A. R.; Huffman, J. C.; Zaleski, J. M. *Inorg. Chem.* **2003**, *42*, 1663–1672.

ancillary phenanthroline ligands are planar to within 0.07 Å, with a dihedral angle of 96° between the two planes. The coordinated bptt ligand is slightly distorted, possessing a bowed structure where the apex corresponds to the pyrazine ring. This distortion is likely a product of the π-stacking interaction observed at the pyrazine ring (3.51 Å between independent molecules) because it is not observed in the gas phase structure optimized at the 3-21G level. The effect of the π-stacking interaction on the bonding within the pyrazine ring is reflected in an increase of the N7−C29 and N8−C32 bond lengths and a corresponding decrease in the C29−C32 and C30−C31 bond lengths relative to their computed values (see Supporting Information, Table S2). A slight decrease in the in the C−C bond order facilitates out-of-plane distortions at the pyrazine ring, leading to the bowing of the bptt ligand observed in the X-ray structure.

Electronic Structure. Both bptt derivatives show intense $\pi\pi^*$ transitions at $\lambda \sim 395$ nm and a weak $n\pi^*$ feature centered at $\lambda \sim 460$ nm (Figure 2a). The $\lambda = 393$ nm peak ($\varepsilon_{393} = 33{,}000$ M^{-1} cm^{-1}) in **1** is red-shifted to $\lambda = 398$ nm in **2** by incorporation of a *tert*-butyl group at the *para* position of the terminal phenyl ring ($\varepsilon_{398} = 33{,}200$ M^{-1} cm^{-1}), while the weaker features centered at $\lambda \sim 460$ nm do not mirror this effect. Free ligands **1** and **2** show notably strong fluorescence at room temperature, with $\lambda_{max} = 423$ and 439 nm, respectively. The shift loosely correlates to the changes in the absorption spectrum of the ligand upon substitution. A parallel red-shift is also observed in the 77 K phosphorescence spectra of **1** and **2** where the maxima of $\lambda = 531$ and 568 nm for **1** are shifted to $\lambda = 535$ and 575 nm for **2**. These observations indicate that the frontier molecular orbitals of **1** and **2** have significant character on the terminal phenyl groups, while the weaker $n\pi^*$ features are predominantly localized on the pyrazine ring.

Support for this interpretation derives from time-dependent density functional theory (TDDFT) calculations (Figure 3). The lowest energy allowed electronic transitions calculated for **1** involve π and π^* orbitals primarily localized on the pyrazine, dialkynyl, and terminal phenyl groups. Excitation of these transitions leads to antibonding character at the alkynes and within the pyrazine ring. From the density plots, it is clear that there is a much larger contribution from the *para* position of the terminal phenyl groups in the HOMO and SHOMO than in the LUMO and SLUMO. Substitution of a strong σ-donor group at this position should therefore destabilize the HOMO and have a similar, but smaller, effect on the LUMO energy, resulting in a small red shift of the electronic transition. A red shift of the $\lambda \sim 395$ nm transition is indeed observed upon substitution (Figure 2a) indicating that the TDDFT result is consistent with the electronic spectra of **1** and **2** in solution.

The electronic absorption spectra of **3** and **4** have two prominent low energy features; a ligand-centered transition at $\lambda \sim 395$ nm and metal-to-ligand charge transfer transition at $\lambda \sim 450$ nm (Figure 2b). The red-shift in the $\lambda \sim 395$ nm feature observed in the electronic spectra of **1** and **2** upon *tert*-butyl substitution (Figure 2a) is retained between complexes **3** and **4** (Figure 2b). These ligand-centered transitions also appear to gain intensity (**3**: $\varepsilon_{387} = 41{,}500$ M^{-1} cm^{-1}, **4**: $\varepsilon_{394} = 42{,}100$ M^{-1} cm^{-1}), but this is a result of overlap with the Ru(dπ)-to-phen(π^*) charge-transfer transitions and the underlying Ru^{2+} *d-d* bands that also occur in this energy region.[89] Surprisingly, the primary charge transfer transition at $\lambda \sim 450$ nm remains largely unaffected by the substitution at the terminal phenyl rings. Given the effect of *tert*-butyl substitution on the lowest energy $\pi-\pi^*$ transition in **1** and **2**, one would expect a

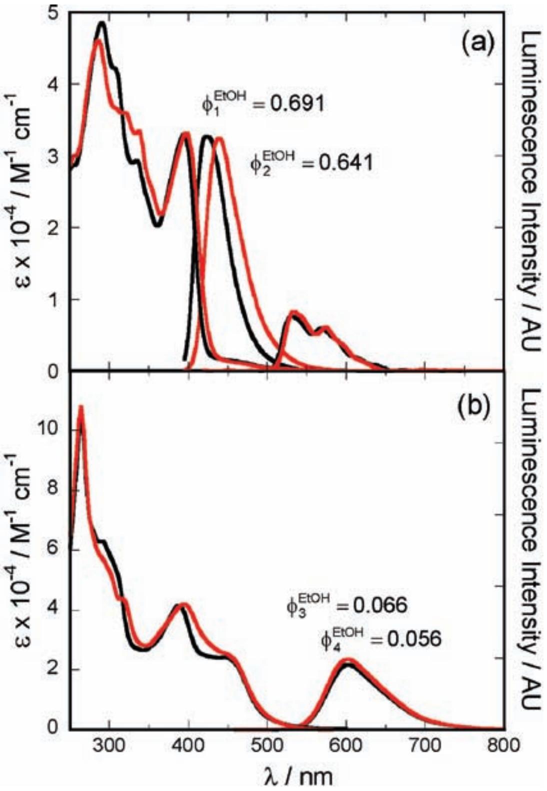

Figure 2. Electronic absorption and emission spectra for **1**−**4** collected in ethanol. (a) 298 K absorption and fluorescence ($\lambda_{ex} = 395$ nm, $\lambda_{em} \sim 420$ nm) spectra and 77 K phosphorescence ($\lambda_{ex} = 395$ nm, $\lambda_{em} \sim 530$ nm) for **1** (black) and **2** (red). (b) 298 K absorption and luminescence ($\lambda_{ex} = 450$ nm, $\lambda_{em} \sim 600$ nm) spectra for **3** (black) and **4** (red). Fluorescence (ϕ_1 and ϕ_2) and luminescence (ϕ_3 and ϕ_4) quantum yields for **1**−**4** are shown above the emission profiles.

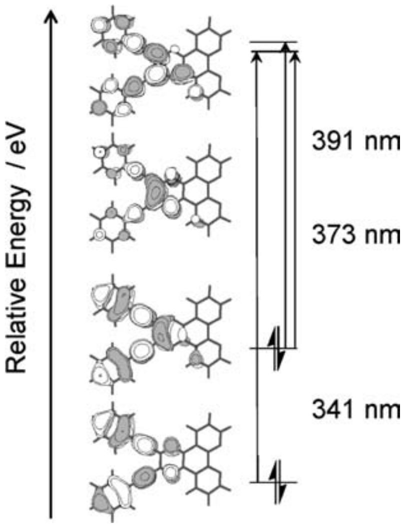

Figure 3. TDDFT description of the frontier molecular orbitals of **1**.

---

[89] Juris, A.; Balzani, V.; Barigelletti, F.; Campagna, S.; Belser, P.; Von Zelewsky, A. *Coord. Chem. Rev.* **1988**, *84*, 85–277.

Table 1. Vibrational Assignments from Density Functional Theory and Experimental Resonance Raman Shifts for **3**

ν	assignment[a]	B3LYP/3-21G//LANL2DZ (cm^{-1})[b]	B3LYP/3-21G//LANL2DZ (cm^{-1})[c]	Raman shift (cm^{-1}) λ_{ex} = 457. Nine nm	Raman shift (cm^{-1}) λ_{ex} = 406.7 nm
80	alkyne oop-wag	620	588		590
89	phenyl breathe	684	649		654
96	bptt-phen breathe	749	711		708
100	ancillary-phen breathe	761	723	727	725
112	ancillary-phen H-oop wag	840	798	805	
122	ancillary-phen breathe	933	886	883	
166	pyrazine breathe	1128	1071		1070
175	ancillary-phen breathe	1227	1165	1166	1165
187	bptt-phen C−C stretch	1260	1197		1211
189	ancillary-phen C−N stretch	1287	1222		1221
198	ancillary-phen C−C stretch	1327	1260	1269	
199	bptt-phen C−C stretch	1339	1272		1272
203	ancillary-phen C−C stretch	1378	1309	1319	
206	pyrazine C−N stretch	1417	1346		1349
222	bptt-phen C−C stretch	1515	1438		1435
226	ancillary-phen C−C stretch	1536	1458	1457	
238	bptt-phen C−C stretch	1599	1519		1568
240	ancillary-phen C−C stretch	1609	1528	1572	
241	ancillary-phen C−C stretch	1610	1529	1599	
242	phenyl C−C stretch	1626	1544		1595
246	alkyne stretch	2321	2204	2204	2204

[a] Assignments represent the region of the molecule with the greatest atomic displacement. [b] Unscaled values. [c] Scaled by 0.9496.

corresponding shift in the MLCT transitions of **3** and **4** if the ligand LUMO is delocalized about the bptt π-system. Additionally, given the low reduction potential reported for **3** (−1.14 V vs Fc/Fc$^+$),[64] a significantly red-shifted MLCT transition relative to the $[Ru(bpy)_3]^{2+}$ and $[Ru(phen)_3]^{2+}$ derivatives would be expected.[89,90] The absence of a shift in the MLCT transition upon *tert*-butyl substitution suggests that **3** and **4** have bichromophoric character, similar to $[Ru(phen)_2dppz]^{2+}$ and derivatives thereof.[47,52,91−94] This is most clearly depicted by the DFT description of the frontier orbitals of **1** (Figure 3), which indicates that the bptt ligand is composed of two non-degenerate π-systems where the LUMO and SLUMO are primarily localized on the pyrazine, dialkynyl, and terminal phenyl groups, while the phenanthroline π*-orbitals lie higher in energy. Although it might be expected that the phen-based π*-orbitals of **1** and **2** would be sufficiently stabilized by complexation to facilitate communication between these two π-systems,[47] this effect is not apparent in the ground-state electronic absorption spectra of **3** and **4**.

The bichromophoric description of the electronic structure derived from the electronic spectrum of **3** (Figure 2b) is consistent with the ground-state resonance Raman spectra, and corresponding DFT vibrational assignments (Table 1). Generally, vibrational modes associated with the bptt ligand are enhanced upon λ_{ex} = 406.7 nm, while vibrations associated with the ancillary phenanthrolines are enhanced with λ_{ex} = 457.9 nm (Table 1). With λ_{ex} = 457.9 nm excitation, the modes at 1457, 1572, and 1599 cm^{-1} associated with the ancillary phenanthrolines all show significant enhancement, while bptt modes such as the alkyne stretch at 2204 cm^{-1} show very low intensity (Figure 4b). Conversely, with λ_{ex} = 406.7 nm, vibrations associated with the bptt ligand (ν_{89}, ν_{189}, ν_{246}) dominate the vibrational spectrum (Figure 4a). This includes modes associated with the phenanthroline (ν_{96}, ν_{199}, ν_{222}, and ν_{238}), the pyrazine-dialkynyl (ν_{80}, ν_{166}, ν_{206}, and ν_{246}), and the terminal phenyl (ν_{89} and ν_{242}) fragments of the bptt ligand.

Enhancement of vibrations distributed throughout the bptt ligand upon λ_{ex} = 406.7 nm excitation implies an electronic structure of the coordinated ligand that is perturbed significantly from that described in Figure 3. Specifically, the Raman spectrum suggests that the electronic transition at $\lambda \sim 395$ nm in **3** is composed of a more extensively delocalized orbital involving both the phenanthroline and the pyrazine-dialkynyl portions of the ligand. A more delocalized orbital may derive from stabilization of the phenanthroline-centered π* orbitals of bptt upon complexation which facilitates a mixing of the non-degenerate phenanthroline and pyrazine-dialkynyl orbitals. Such delocalization would result in a red-shift of the MLCT transition relative to the electronic spectrum of $[Ru(bpy)_3]^{2+}$. This is clearly not observed in the ground-state electronic absorption spectrum of **3** (Figure 2b). The enhancement pattern in the λ = 406.7 nm Raman spectrum most likely derives from a degeneracy of two distinct electronic transitions (ππ* bptt-pyrazine/dialkynyl-centered and Ru(dπ)-bptt(π*)) which results in detection of vibrations from both fragments of the bptt ligand.

To a first approximation, the room temperature emission spectra of the ruthenium complexes **3** and **4** demonstrate behavior comparable to most ruthenium polypyridine derivatives upon MLCT excitation (Figure 2b).[89] The emission maxima (λ = 603 nm for **3** and **4**) and quantum yields of **3** (ϕ = 0.066) and **4** (ϕ = 0.056) are relatively unaffected by substitution at the terminal phenyl of the bptt ligand and are similar to those reported for $[Ru(phen)_3]^{2+}$ (λ = 604 nm, ϕ = 0.058).[66] In contrast, the room temperature lifetimes (τ_3 = 630 ns, τ_4 = 590 ns) are significantly

---

(90) Balzani, V.; Credi, A.; Venturi, M. *Coord. Chem. Rev.* **1998**, *171*, 3–16.

(91) Ackermann, M. N.; Interrante, L. V. *Inorg. Chem.* **1984**, *23*, 3904–3911.

(92) Amouyal, E.; Homsi, A.; Chambron, J. C.; Sauvage, J. P. *J. Chem. Soc., Dalton Trans.* **1990**, 1841–1845.

(93) Chambron, J. C.; Sauvage, J. P.; Amouyal, E.; Koffi, P. *Nouv. J. Chim.* **1985**, *9*, 527–529.

(94) Fees, J.; Ketterle, M.; Klein, A.; Fiedler, J.; Kaim, W. *J. Chem. Soc., Dalton Trans.* **1999**, 2595–2600.

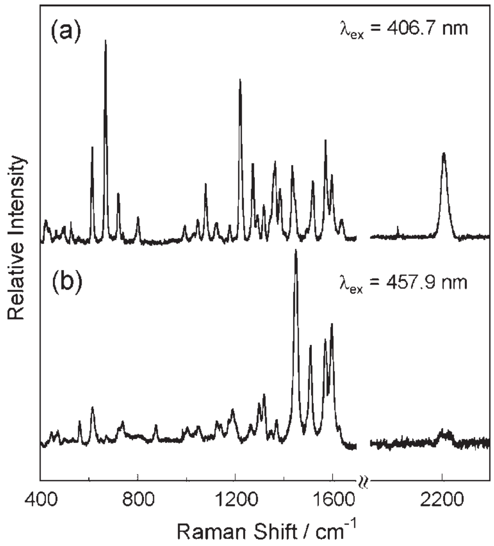

Figure 4. Resonance Raman spectra of **3** collected at 298 K in DMSO (20 mM) with (a) λ_{ex} = 406.7 nm, and (b) λ_{ex} = 457.9 nm.

shorter than those reported for $[Ru(phen)_3]^{2+}$ ($\tau \sim 1.0\,\mu s$).[89] This discrepancy implies quenching by the bptt ligand, similar to what is observed for $[Ru(phen)_2dppz]^{2+}$ in polar or H-bonding solvents.[42,89] Both **3** and **4** are structurally and electronically related to $[Ru(phen)_2dppz]^{2+}$, as they possess two non-degenerate low-energy electronic transitions.

The transient absorption spectra of **3** and **4** also imply an influence of the bptt ligand on the nature of the lowest-lying excited state (Figure 5). The transient absorption spectral features for **3** and **4** decay with the same lifetime as the luminescence decay (τ_3 = 650 ns and τ_4 = 600 ns) and are generally similar to those observed for $[Ru(bpy)_3]^{2+}$.[92,95] Photoexcitation (λ_{ex} = 450 nm) of **3** leads to bleaching of both the MLCT and the ligand-centered transitions at $\lambda \sim 450$ nm and $\lambda \sim 390$ nm, and an increase in the OD at $\lambda \sim 345$ nm. For **4**, the $\lambda \sim 345$ nm peak and the $\lambda \sim 390$ nm bleach show a ~ 5 nm red-shift upon *tert*-butyl substitution, similar to the trend observed in the ground state absorption spectra of **1**−**4**. The primary difference between the literature transient absorption spectra for $[Ru(bpy)_3]^{2+}$ and spectra for **3** and **4** is the position of the positive feature at $\lambda \sim 345$ nm, which is significantly blue-shifted relative to $[Ru(bpy)_3]^{2+}$ ($\lambda \sim 375$ nm). This shift is likely related to the bleach at $\lambda \sim 390$ nm which influences the observed maximum of the positive feature at $\lambda \sim 375$ nm in $[Ru(bpy)_3]^{2+}$. Given these spectral differences and the quenched lifetimes of **3** and **4** relative to $[Ru(bpy)_3]^{2+}$, it is apparent that the emissive state (or states)[96,97] has character that extends out to the terminal phenyl groups of the bptt ligand.

Interactions with DNA. Given the structural and electronic similarities of **3** and **4** to widely studied $[Ru(phen)_2dppz]^{2+}$, we have focused our investigations on the electronic effects of DNA binding on the emission energies and lifetimes of **3** and **4** in an aqueous environment. Similar to the electronic absorption spectrum in ethanol, the spectrum of **3** in an aqueous environment contains two low-energy transitions at $\lambda \sim 450$ nm and $\lambda \sim 390$ nm (Figure 6a). The primary spectral difference between the two conditions (i.e., in ethanol and in water) is the marked decrease in the intensity of the 390 nm transition (ε_{max} = 29,100 M^{-1} cm^{-1}), as well as a slight red-shift of the peak maximum (λ_{max} = 395 nm). Similar changes are observed for the *tert*-butyl derivative, **4**, although the decrease in intensity and red-shift of the band maximum results in significant spectral overlap between the ligand-centered and MLCT transitions, and thus poor resolution of these spectral features (Figure 6b). In addition to the changes in the absorption spectrum, the emission spectra of both **3** and **4** are significantly red-shifted (**3**: λ_{em} = 634 nm; **4**: λ_{em} = 634 nm) and dramatically quenched, similar to what is observed for $[Ru(phen)_2dppz]^{2+}$.[42,45]

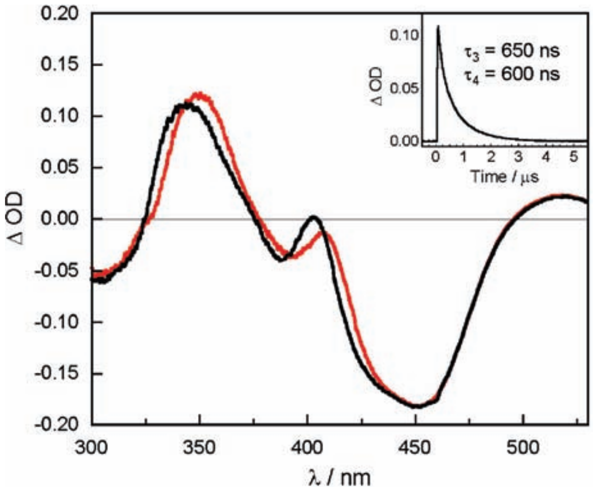

Figure 5. Transient absorption spectra of **3** (black) and **4** (red) collected between 50 and 150 ns after laser excitation (λ_{ex} = 450 nm) in ethanol at 298 K. Inset: Change in optical density of **3** at 350 nm after λ_{ex} = 450 nm.

Addition of 10 mol equiv (nucleobase) of CT-DNA to a solution of **3** induces a decrease in the intensity and a red shift of the 395 nm transition (λ_{max} = 400 nm, ε_{max} = 26,400 M^{-1} cm^{-1}), concurrent with a 9-fold increase in the luminescence quantum yield (Figure 6a). These effects are similar to the spectral signatures of intercalation for $[Ru(phen)_2dppz]^{2+}$ and related complexes.[9,33,83,98] In contrast to **3**, **4** demonstrates only minor changes in both the electronic absorption and the emission spectra upon addition of CT-DNA (Figure 6b), suggesting *tert*-butyl substitution at the terminal phenyl dramatically decreases the ability of **4** to intercalate between the DNA base pairs. Additionally, the relatively modest increase in luminescence quantum yield for **3** relative to dppz ($> 10^4$)[33] reveals that the intercalation of **3** occurs via π-stacking involving the terminal phenyl groups, leaving the pyrazine portion of the molecule partially accessible for solvent quenching.

The intrinsic luminescence of **3** can be monitored to quantitatively evaluate its binding affinity for DNA in aqueous buffer relative to $[Ru(phen)_2dppz]^{2+}$. Relatively high salt concentrations (200 mM NaCl and 10 mM $MgCl_2$) were employed to discourage non-specific electrostatic binding. The emission maximum (λ_{em} = 600 nm) is red-shifted relative to that of **3** in Tris-HCl buffer with

---

[95] Bensasson, R.; Salet, C.; Balzani, V. *J. Am. Chem. Soc.* **1976**, *98*, 3722–3724.

[96] Hager, G. D.; Crosby, G. A. *J. Am. Chem. Soc.* **1975**, *97*, 7031–7037.

[97] Sykora, M.; Kincaid, J. R. *Inorg. Chem.* **1995**, *34*, 5852–5856.

[98] Hartshorn, R. M.; Barton, J. K. *J. Am. Chem. Soc.* **1992**, *114*, 5919–5925.

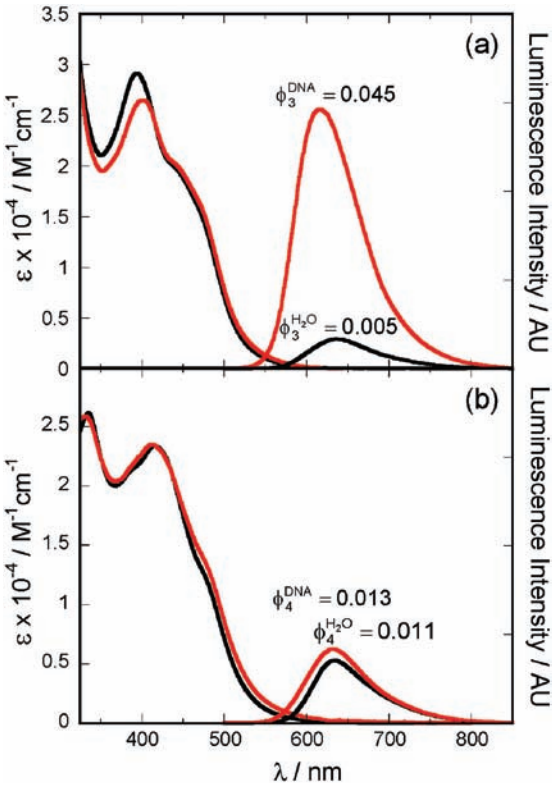

Figure 6. Electronic absorption and emission (λ_{ex} = 450 nm) spectra of **3** (a) and **4** (b) in the absence (black) and presence (red) of 10 mol equiv (nucleobase) CT-DNA in 10 mM Tris-HCl at pH 7.2 and 298 K. Luminescence quantum yields for **3** and **4** in the absence ($\phi^{\mathrm{H}}{}_2{}^{0}$) and presence ($\phi^{\mathrm{DNA}}$) of DNA are shown above the emission profiles.

no added salts (λ_{em} = 615 nm). The emission intensity at λ = 600 nm after excitation at λ = 399 nm was used to construct a DNA binding curve (Figure 7). The luminescence intensity increases by a factor of nearly 10 over the course of the experiment, consistent with the previous increase observed for the 10-fold excess CT-DNA measurement. This is accompanied by a small shift of the emission maxima (~5 nm) to longer wavelength. Fitting the binding isotherm to a simple one site binding model on a per base pair basis with no additional assumptions yields a binding association constant (K_b) of 3.3 ± 0.2 × 10^4 M^{-1}. The strength of this interaction in relatively high salt concentration indicates the binding is intercalative. This K_b is in good agreement with those reported for other molecular light switch complexes which range from 10^4 to 10^7 M^{-1}.[28,33,36,99] Specifically, the K_b was determined to be 4.95 × 10^6 M^{-1} for $[Ru(phen)_2dppz]^{2+}$ and 8.4 × 10^5 M^{-1} for $[Ru(bpy)_2taptp]^{2+}$ by following spectral changes in the electronic absorption profile upon DNA binding.[36] Since the bptt ligand is bulkier and less planar than either of these ligands, one would expect to observe a lower affinity intercalative interaction.

The luminescence lifetimes of **3** and **4** in an aqueous environment both demonstrate biphasic kinetics (**3**: τ_1 = 40 ns, τ_2 = 230 ns; **4**: τ_1 ~ 26 ns, τ_2 = 150 ns) with significantly reduced lifetimes relative to $[Ru(phen)_3]^{2+}$ (Figures 8a and 8c). Upon addition of DNA, the luminescence lifetime of **3** increases considerably (τ_1 = 220 ns, τ_2 = 990 ns), but retains biphasic decay kinetics (Figure 8b).

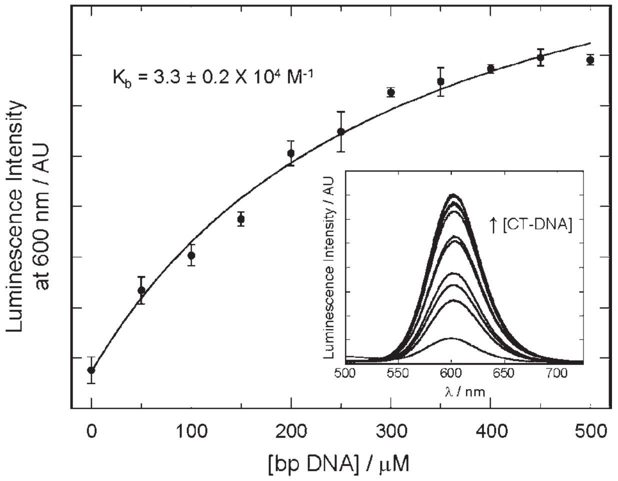

Figure 7. Binding isotherm for **3** binding to CT-DNA determined by intrinsic luminescence at 600 nm (λ_{ex} = 399 nm). Inset: Representative luminescence emission spectra of **3** as a function of increasing CT-DNA.

The decay kinetics of the transient absorption at λ = 350 nm of **3** in the presence of DNA are also biexponential (τ_1 = 210 ns, τ_2 = 1000 ns) and possess rate constants that closely parallel those observed for the excited state decay by emission (Figure 8b). In contrast to **3**, the lifetime of **4** increases only slightly upon addition of DNA (τ_1 = ~29 ns, τ_2 = 260 ns) (Figure 8d), a result that is consistent with the small change observed in the luminescence quantum yield under the two solution conditions.

The excited state model of $[Ru(phen)_2dppz]^{2+}$ luminescence decay describes two distinct ^{3}MLCT excited states; a $^3MLCT_{phen}$ state, where the negative charge is delocalized about phenanthroline components of the three ligands, and a lower-energy $^3MLCT_{phzn}$ state, where the negative charge resides primarily on the phenazine portion of the dppz ligand.[31,39,41,45,46] Ultrafast time-resolved emission and resonance Raman experiments have demonstrated that there is rapid interconversion between these two states, and they likely establish an equilibrium condition in less than 20 ps.[41,45,49] The energy of the $^3MLCT_{phzn}$ state is highly sensitive to solvent interactions at the pyrazine nitrogens. In polar or H-bonding solvents, the $^3MLCT_{phzn}$ state is stabilized sufficiently to significantly deactivate the $^3MLCT_{phen}$ state leading to a dramatically reduced luminescence lifetime relative to $[Ru(phen)_3]^{2+}$. In water, $[Ru(phen)_2dppz]^{2+}$ exhibits emission from the $^3MLCT_{phen}$ state at λ ~ 630 nm and weak emission from the $^3MLCT_{phzn}$ state in the near-IR (λ ~ 800 nm).[45] If the phenazine-based MLCT state of **3** ($^3MLCT_{bptt}$) were emissive, it would be expected to appear at lower energy than the analogous state in $[Ru(phen)_2dppz]^{2+}$ because of the extended conjugation and to have an even lower quantum yield since its reduced rigidity leads to increased non-radiative decay. However, for **3** and **4**, only a single emission band corresponding to the $^3MLCT_{phen}$ excited state is observed and no emission features are present between 700 and 1200 nm. Even though the $^3MLCT_{bptt}$ state is non-emissive and does not contribute to the observed dual emission, it is responsible for the light switch effect for **3** upon DNA binding.

Though $[Ru(phen)_2dppz]^{2+}$ displays biphasic decay kinetics when bound to DNA, the decay is monoexponential in water. From studies on the luminescence lifetimes of

---

(99) Pyle, A. M.; Rehmann, J. P.; Meshoyrer, R.; Kumar, C. V.; Turro, N. J.; Barton, J. K. *J. Am. Chem. Soc.* **1989**, *111*, 3051–3058.

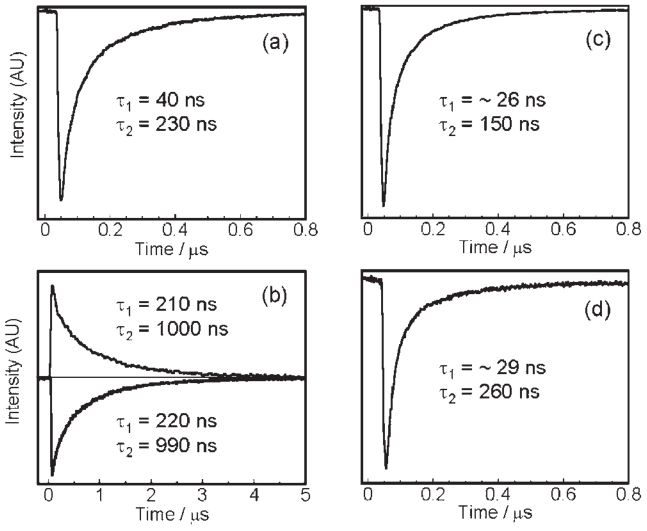

Figure 8. Kinetic profiles of the excited state decay of **3** and **4** in the presence and absence of 10 mol equiv (nucleobase) CT-DNA in 10 mM Tris-HCl at pH 7.2 and 298 K after λ_{ex} = 450 nm. (a) Luminescence decay of **3** at λ = 625 nm in the absence of DNA. (b) Transient absorbance (λ = 350 nm) and luminescence decay (λ = 625 nm) of **3** in the presence of DNA. (c) Luminescence decay of **4** at λ = 625 nm in the absence of DNA. (d) Luminescence decay of **4** at λ = 625 nm in the presence of DNA.

enantiomerically pure samples of $[Ru(phen)_2dppz]^{2+}$, it has been shown that each enantiomer (Λ and Δ) possesses unique biphasic decay kinetics in the presence of DNA ($\Lambda\tau_w$ = 40 ns, $\Lambda\tau_t$ = 150 ns and $\Delta\tau_w$ = 160 ns, $\Delta\tau_t$ = 850 ns)[100] deriving from differing affinities of the two enantiomers for the handed DNA substrate.[33,100] The biexponential emission decays for *each enantiomer* (Λ or Δ) have been determined to derive from the relative proximity of the intercalated $[Ru(phen)_2dppz]^{2+}$ units.[33] This analysis indicates that the longer lifetime component (τ_t) derives from more closely bound emissive intercalators, which generates a tightly packed DNA-metal complex structure resulting in more efficient solvent shielding of the pyrazine nitrogens.[33] In contrast, emissive intercalators that are widely spaced along the DNA polymer experience a less efficient shielding of the pyrazine nitrogens, and consequently demonstrate a shorter lifetime (τ_w). However, the photophysical behavior of **3** cannot be explained by the same phenomena even though a racemic mixture was employed for binding studies, since it also displays biphasic kinetics in aqueous solution in the absence of DNA where the stereochemistry of the complex would have no effect.

Solvent-Dependent Luminescence. In an effort to further explore this unusual biphasic behavior, the solvent dependence of the emission kinetics of **3** was explored in varying $CH_3CN{:}H_2O$ solvent mixtures. Samples were excited at λ = 447.7 nm, and the emission kinetics were evaluated at 600 nm. As expected, in pure CH_3CN, the lifetime (τ = 1040 ns) is longer than that measured in EtOH, and nearly identical to that of $[Ru(phen)_3]^{2+}$ in CH_3CN (Table 2).[66] In non-hydrogen bonding solvents, there is little quenching because of interactions at the phenazine nitrogens leading the complex to behave like $[Ru(phen)_3]^{2+}$. As CH_3CN is replaced with H_2O in the solvent mixture, increased H-bonding at the phenazine nitrogens causes the lifetimes to decrease (Table 2). When the amount of CH_3CN is reduced to 20% of the solution volume, **3** displays biphasic emission kinetics where the fraction of molecules emitting from the state corresponding to the shorter lifetime (F_1) is 0.23 which is comparable to that fraction in pure H_2O (F_1 = 0.19). The somewhat reduced lifetimes in 20% CH_3CN versus pure H_2O may be due the decreased ability to form H-bonding networks that can stabilize the excited state(s) in the solvent mixture.

Table 2. Luminescence Lifetimes of **3** as a Function of Solvent

% acetonitrile in water	τ_1/ns	τ_2/ns	F_1[a]	R^2[b]
100	1040	n/a	1	0.9998
80	230	n/a	1	0.9994
60	72	n/a	1	0.9994
40	38	n/a	1	0.9993
20	~19	160	0.23	0.993
0	40	230	0.19	0.99

[a] Fractional contribution to luminescence from τ_1. [b] Square of the correlation coefficient for the data fit.

Overwhelmingly, molecules obey Kasha's rule and only appreciably emit from the lowest energy excited state.[101] However, at low temperature, many molecules exhibit biphasic decay profiles since excited states that would be equilibrated at room temperature can be trapped by reducing the temperature. Many of these systems exhibit simultaneous emission from ^{3}MLCT and ligand-based triplet states and are discussed in a comprehensive review by Schmehl et al.[50] Molecules that exhibit biphasic decay kinetics in solution at room temperature have only rarely been reported.[69,102-104] In each case, biphasic luminescence is the result of two emitting excited states with similar energies separated by a kinetic barrier that prevents complete equilibration of the two states resulting in dual emission. Two of these reports involve mixed-ligand Ru(II) diimine complexes. In the first case, Zhang and co-workers synthesized a complex, $[Ru(bpy)_2L]^{2+}$ (where L is 4-methyl-4′-[*p*-(dimethyl-amino)-α-styryl]-2,2′-bipyridine) that displayed dual emission at room temperature.[103] Using time-resolved emission spectra, they were able to resolve two luminescence maxima at different energies and assign the two emitting states as ^{3}MLCT and ^{3}ILCT in nature. In the second example, Tor et al. synthesized a series of alkyne-substituted phen ligands and corresponding mixed-ligand Ru(II) complexes and found those asymmetrically substituted at the 4-position of the phenanthroline have biphasic emission profiles with the fractional contributions from the short- and long-lived components variable with the detection wavelength.[69] The proposed explanation suggests that the ^{3}MLCT state involving the alkyne-substituted phen ligand was not completely equilibrated with the phen-based ^{3}MLCT resulting in emission from both ^{3}MLCT states.

Attempts to isolate the two emitting states in **3** by examining time-resolved emission spectra were largely unsuccessful. A small red-shift in the emission maxima from 600 to 610 nm is observed at long time delays (> 1 µs

---

(100) Erkkila, K. E.; Odom, D. T.; Barton, J. K. *Chem. Rev.* **1999**, *99*, 2777–2795.

(101) Kasha, M. *Faraday Discuss.* **1950**, *9*, 14–19.

(102) Ferraudi, G.; Feliz, M.; Wolcan, E.; Hsu, I.; Moya, S. A.; Guerrero, J. *J. Phys. Chem.* **1995**, *99*, 4929–4934.

(103) Song, L.; Feng, J.; Wang, X.; Yu, J.; Hou, Y.; Xie, P.; Zhang, B.; Xiang, J.; Ai, X.; Zhang, J. *Inorg. Chem.* **2003**, *42*, 3393–3395.

(104) Matsumoto, K.; Matsumoto, N.; Ishii, A.; Tsukuda, T.; Hasegawa, M.; Tsubomura, T. *Dalton Trans.* **2009**, 6795–6801.

Table 3. Temperature Dependence of the Luminescence Lifetimes of **3**

solvent	temperature/K	τ_1/ns	τ_2/ns	F_1[a]	R^2 [b]
EtOH	298	630	n/a	1	0.9998
	233	1510	n/a	1	0.9996
	193	1770	n/a	1	0.9999
	77	4210	n/a	1	0.991
60:40 Ethylene Glycol:H_2O	333	143	~1190	> 0.99	0.999
	298	82	800	0.93	0.9992
	273	61	1120	0.91	0.998
	233	41	1410	0.89	0.999
	77	4980	n/a	1	0.9997

[a] Fractional contribution to luminescence from τ_1. [b] Square of the correlation coefficient for the data fit.

after the laser pulse) for **3** in the presence of DNA in water (λ_{ex} = 447.7 nm) indicating that the two states are nearly degenerate (data not shown). Furthermore, determination of the decay kinetics across the emission spectrum under the same conditions reveals that the luminescence is biphasic at all emission wavelengths, and the lifetimes are independent of wavelength. However, the fractional component F_1 varies across the emission spectrum. Near the emission maximum, F_1 (~ 0.35) is significantly smaller than at wavelengths near the edges of the profile (~ 0.55) (see Figure S6 in Supporting Information). If the sample is excited with λ_{ex} = 396.0 nm into the ligand $\pi\pi^*$ manifold, F_1 is reduced at all wavelengths but most significantly near the emission maximum (see Figure S6 in Supporting Information). This signifies that the second emitting state is likely ligand-based. The two emitting states could not be distinguished in transient absorption experiments because of the similarity of their lifetimes and the poor quantum yield of **3** in water. However, lifetimes of the emitting states are significantly reduced by the presence of oxygen in solution confirming that both states are triplet in nature.

Temperature-Dependent Luminescence. The temperature dependence of emission quantum yields or lifetimes can provide valuable information about the relative energies of multiple excited states. Papanikolas et al. have used the temperature dependence of the quantum yield of $[Ru(phen)_2\text{-}dppz]^{2+}$ to determine the relative energies of the Ru *d-d* excited state and the two ^{3}MLCT excited states that contribute to its photophysical light switching behavior.[37,38] Temperature dependence of radiative and non-radiative decay rate constants have also been used to probe the electronic effects of methyl substitution in substituted $[Ru(phen)_2(dpq)]^{2+}$ and $[Ru(phen)_2(dppz)]^{2+}$ complexes.[105,106] Within this theme, the temperature dependence of the emission kinetics of **3** in various solvent systems has been measured (λ_{ex} = 447.7 nm, λ_{em} = 600 nm) (Table 3). Predictably, the monoexponential emission lifetime of **3** in EtOH increases as the temperature is lowered because of reduced non-radiative decay. At 77 K, the emission decay is also monophasic with a lifetime of 4.2 μs. There are two possible explanations for the origin of the monophasic luminescence decay in EtOH at room temperature: the decay arises either from the isolated ^{3}MLCT excited state or from a kinetic steady state/equilibrium between the ^{3}MLCT and the ligand localized $^3\pi\pi^*$ state on a time scale faster than the luminescence.[50] To distinguish between the two possibilities, uncoordinated ligand **1** was triplet sensitized at room temperature to estimate the energy of the $^3\pi\pi^*$ state. Under this condition, strong phosphorescence from **3** is observed. Comparison of the luminescence of **3** (λ_{ex} = 450 nm) with that of **1** sensitized with xanthone (λ_{ex} = 355 nm, τ = 6.36 μs) reveals that at room temperature, the energy profile of the $^3MLCT_{phen}$ state is nearly identical to the energy profile of the $^3\pi\pi^*_{bptt}$ state, with both displaying maxima at ~600 nm (Figure 9). Since these two states are both triplet in nature and nearly degenerate, some degree of wave function mixing occurs leading to state coupling and the potential for rapid kinetic interconversion. The phosphorescence of **1** at 77 K also shows vibrational fine-structure with two distinct vibronic progressions (ΔE ~1275 cm^{-1}) corresponding to the energy of the C−C and C−N stretching modes of the aromatic rings.[107] The vibrational signatures are consistent with those observed in the 77 K emission spectrum of **3** (ΔE ~ 1225 cm^{-1}), suggesting that the luminescence may be partially ligand in origin (Figure 9). The observation is also similar to other Ru(II) diimine complexes that display vibrational fine-structure with energies of 1050−1350 cm^{-1}.[66,96]

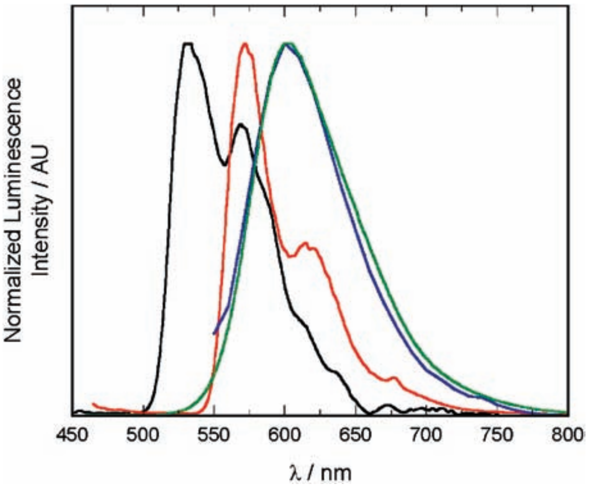

Figure 9. Triplet emission spectra in EtOH of **1** at 77 K (black), **3** at 77 K (red), **1** triplet sensitized with xanthone at room temperature (RT; blue), and **3** at RT (green).

To evaluate the luminescence of **3** in aqueous solution over a larger temperature range, a 60:40 ethylene glycol: H_2O solvent mixture was chosen. As the temperature is raised from 233 to 333 K, the lifetime of the short-lived state increases while the lifetime of the long-lived state decreases. Concomitantly, the fraction of the emission from the short-lived state increases (Table 3), and is readily visible in the emission decay curves (Figure 10). At 333 K, the luminescence is nearly monoexponential with > 99% of the emission arising from the short-lived $^3MLCT_{phen}$ excited state. At room temperature, however, the luminescence trace is biphasic, illustrating that the rate of interconversion between the $^3MLCT_{phen}$ and $^3\pi\pi^*_{bptt}$ states is of the same order of magnitude as their luminescence decay

---

(105) O'Donoghue, K.; Penedo, J. C.; Kelly John, M.; Kruger Paul, E. *Dalton Trans.* **2005**, 1123–1128.

(106) Olofsson, J.; Wilhelmsson, L. M.; Lincoln, P. *J. Am. Chem. Soc.* **2004**, *126*, 15458–15465.

(107) Campagna, S.; Puntoriero, F.; Nastasi, F.; Bergamini, G.; Balzani, V. *Top. Curr. Chem.* **2007**, *280*, 117–214.

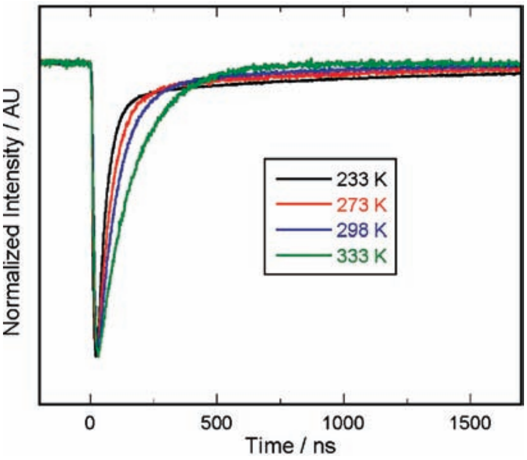

Figure 10. Kinetic profiles of the excited state luminescence decay of **3** in 60:40 ethylene glycol:H_2O at 233 K (black), 273 K (red), 298 K (blue), and 333 K (green).

rates. This further suggests that the two states are only moderately coupled with some appreciable inter-state barrier. At lower temperatures in aqueous solution, there is sufficient thermal energy for some fraction of molecules to traverse the barrier to the ligand-localized $^3\pi\pi^*_{\text{bptt}}$ state, but the higher kinetic barrier to the reverse rate retards back-population of the $^3\text{MLCT}_{\text{phen}}$ state. Consequently, the fractional emission from the $^3\pi\pi^*_{\text{bptt}}$ state (F_2) is slightly larger at lower temperature ($F_2 = 0.07$ at 298 K, $F_2 = 0.11$ at 233 K). Thus, the lower energy $^3\pi\pi^*_{\text{bptt}}$ state effectively quenches the $^3\text{MLCT}_{\text{phen}}$ state resulting in a reduced luminescence lifetime for the $^3\text{MLCT}_{\text{phen}}$ component of the emission. Meanwhile, the lifetime of the $^3\pi\pi^*_{\text{bptt}}$ state increases as the temperature is lowered because of reduced non-radiative deactivation. Interestingly, at 77 K, the emission is purely monophasic since excitation ($\lambda_{\text{ex}} = 447.7$ nm) leads to a thermally trapped $^3\text{MLCT}_{\text{phen}}$ state that is no longer able to access the $^3\pi\pi^*$ bptt excited state. The lifetime of **3** at 77 K in 60:40 ethylene glycol:H_2O ($\tau = 5.0\,\mu$s) is similar to that of **3** ($\tau = 4.2\,\mu$s) and $[\text{Ru(bpy)}_2\text{dppz}]^{2+}$ ($\tau = 4.8\,\mu$s) at 77 K, but somewhat quenched relative to $[\text{Ru(phen)}_3]^{2+}$ ($\tau = 9.9\,\mu$s) because of deactivation by the dark $^3\text{MLCT}_{\text{phzn}}$ state.[38,66] In contrast, as the temperature is raised, the complex gains sufficient thermal energy to overcome the inter-state electronic barrier and the $^3\text{MLCT}_{\text{phen}}$ and $^3\pi\pi^*_{\text{bptt}}$ excited states increasingly equilibrate. At 333 K, the two states are almost completely equilibrated giving rise to the essentially monoexponential luminescence decay kinetics ($\tau = 143$ ns).

Excited State Structural Model. The excited state photophysics and dynamics model for **3** follows from the established electronic paradigms for both $[\text{Ru(phen)}_2\text{dppz}]^{2+}$[31,39–41,45,46,108] and $[\text{Re(dppz)(CO)}_3\text{L}]$ analogues[51,52] where two ^{3}MLCT states (phenathroline- and phenazine-based) and a $^3\pi\pi^*$ state control the observed light switch behavior and photophysics. From the temperature dependence of $[\text{Ru(phen)}_2\text{dppz}]^{2+}$ emission in solvents of different polarity, Meyer et al. have shown that the lowest lying $^3\text{MLCT}_{\text{phzn}}$ state is charge-separated in nature, while the $^3\pi\pi^*$ state of dppz lies to higher energy (~540 nm; $\tau \sim 10\text{s}\,\mu$s) and does not contribute to the observed luminescence.[38]

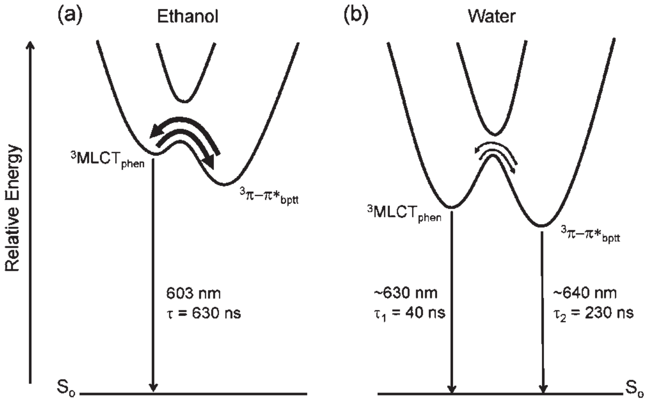

Figure 11. Relative energy level diagram of the interactions between the phenanthroline-based ^{3}MLCT excited state and the ligand-based $^3\pi-\pi^*$ excited state for **3** in ethanol (a) and water (b).

In contrast, *fac*-$[\text{Re(dppz)(CO)}_3\text{Cl}]$ exhibits $^3\pi\pi^*$ ligand-based luminescence at 77 K and ^{3}MLCT luminescence at room temperature, and chloride substitution with triphenylphosphine leads exclusively to luminescence from the $^3\pi\pi^*$ state at both 77 K and room temperature.[52] Resonance Raman studies have shown that the $^3\pi\pi^*$ state is lower in energy for both complexes, but in the case of *fac*-$[\text{Re(dppz)(CO}_3)\text{Cl}]$ the two states are nearly degenerate such that the ^{3}MLCT state is thermally back-populated at room temperature. Since the radiative and non-radiative kinetics of the ^{3}MLCT are much faster than the ligand-based triplet state, the emissive ^{3}MLCT state dominates the observed luminescence as predicted by inter-state conversion kinetics.[50] Additionally, picosecond time-resolved infrared spectroscopy shows that the relative population of the two states in *fac*-$[\text{Re(dppz)(CO}_3)\text{Cl}]$ is solvent dependent, and if electron-withdrawing substituents are added to the dppz ligand, population of the $^3\pi\pi^*$ state is no longer observed because of lowering of the dark state energy.[51]

The photophysics of **3** are encompassed by this general model. Three excited states lead to the observed luminescence behavior, two ^{3}MLCT states and the $^3\pi\pi^*_{\text{bptt}}$ ligand-based state that lies to lower energy and plays an important role in the observed photophysical behavior. From emission and triplet-sensitized phosphorescence measurements of **1**, the $^3\text{MLCT}_{\text{phen}}$ and $^3\pi\pi^*_{\text{bptt}}$ states of **3** are of similar energies ($\lambda \sim 600$ nm), but the $^3\text{MLCT}_{\text{bptt}}$ state is significantly lower in energy ($\lambda > 800$ nm) and exhibits no detectable emission. Consequently, it is the interactions between the $^3\text{MLCT}_{\text{phen}}$ and $^3\pi\pi^*_{\text{bptt}}$ states that give rise to the unique solvent- and temperature-dependent luminescence behavior of **3** (Figure 11). Chelation of the bptt ligand to Ru(II) shifts the $^3\pi\pi^*_{\text{bptt}}$ state slightly to lower energy ($\lambda_{\text{em}} \sim 620$ nm) relative to the free ligand upon triplet sensitization ($\lambda_{\text{max}} = 600$ nm). When solvated in ethanol at room temperature, the $^3\text{MLCT}_{\text{phen}}$ and $^3\pi\pi^*_{\text{bptt}}$ states are strongly coupled, and the small barrier between them leads to rapid interconversion (Figure 11a). The observed emission maximum ($\lambda_{\text{em}} = 603$ nm) and monoexponential lifetime ($\tau = 630$ ns) of **3** indicate that the primary luminescence derives from the $^3\text{MLCT}_{\text{phen}}$ state that is perturbed by the presence of the $^3\pi\pi^*_{\text{bptt}}$ state close in energy. This is consistent with the fact that the $^3\text{MLCT}_{\text{phen}}$ state has a lifetime that is approximately an order of magnitude shorter than that of the $^3\pi\pi^*_{\text{bptt}}$ state ($\tau = 6.6\,\mu$s at room temperature), and suggests that the

---

(108) Coates, C. G.; Jacquet, L.; McGarvey, J. J.; Bell, S. E. J.; Al-Obaidi, A. H. R.; Kelly, J. M. *J. Am. Chem. Soc.* **1997**, *119*, 7130–7136.

rate of interconversion between the two states is more rapid than decay to ground state.

In an aqueous environment, the ^{3}MLCT$_{\mathrm{phen}}$ and the $^3\pi\pi^*_{\mathrm{bptt}}$ states are both stabilized relative to their energies in ethanol. The charge-separated ^{3}MLCT$_{\mathrm{phen}}$ excited state experiences a larger stabilization of ~800 cm^{-1} that is consistent with that observed for the ^{3}MLCT$_{\mathrm{phen}}$ excited state of [Ru(phen)$_2$dppz]$^{2+}$.[9,45,47] The dielectric stabilization reduces the energy gap between the ^{3}MLCT$_{\mathrm{phen}}$ and $^3\pi\pi^*_{\mathrm{bptt}}$ states, and combined with the enhanced reorganizational energy in water, increases the activation barrier between the two states. The increased thermal barrier does not allow rapid interconversion at room temperature (Figure 11b). As the rate of interconversion slows and approaches the rate of radiative decay, emission from both excited states results. The energies of the ^{3}MLCT$_{\mathrm{phen}}$ and $^3\pi\pi^*_{\mathrm{bptt}}$ states correspond to approximately 610 and 620 nm, respectively, when bound to DNA ($\lambda_{\mathrm{em}} = 615$ nm) based on the measured shift in the time-resolved luminescence making the energy gap between the two states ~260 cm^{-1}. If the energy gap between the states is approximately the same in water ($\lambda_{\mathrm{em}} = 634$ nm), the two states would correspond to emission wavelengths of ~630 and 640 nm. In a complementary approach, the energy gap can be estimated from the temperature dependence of the luminescence by using the Boltzmann distribution, and approximating the population of each state by the observed luminescence intensity.[109−112] In this case, since only one emission band is observed, the fractional components of the emission lifetimes were used as an estimate of the populations. A plot of $\ln(F_1/F_2)$ versus $1/T$ was constructed, and the slope was used to get a rough estimate of the energy gap. The energy gap was found to be ~350 ± 100 cm^{-1} in 60:40 ethylene glycol/H$_2$O, which is similar to the estimate from the time-resolved emission data of **3** bound to DNA (see Supporting Information, Figure S7). The dual emission behavior suggests a higher kinetic barrier in H$_2$O relative to ethanol is due to a larger solvent reorganizational energy during conversion from the polar, charge-separated ^{3}MLCT state to the ligand-localized $^3\pi\pi^*_{\mathrm{bptt}}$ state. This is consistent with Ru(II) diimine complexes that show deviations from the energy gap law in protic solvents, and in particular H$_2$O, because of the large reorganizational energy.[113−115] At 77 K in aqueous solution, the rate of interconversion between the two states is slow in part because the high barrier and thermal trapping in the ^{3}MLCT$_{\mathrm{phen}}$ state occurs leading to monoexponential luminescence kinetics.

Summary and Implications

The photophysical properties of **3** and **4** in ethanol resemble those of [Ru(phen)$_3$]$^{2+}$, indicating that traditional MLCT emission is operative and only sparingly affected by the extended conjugation of the bptt framework. In an aqueous environment, **3** and **4** possess notably small luminescence quantum yields consistent with non-radiative solvent quenching at the phenazine nitrogen lone pairs. Moreover, addition of CT-DNA to an aqueous solution of **3** causes a significant increase in the luminescence quantum yield while the quantum yield of **4** is relatively unaffected indicating that *tert*-butyl substitution on the terminal phenyl groups inhibits the ability of **4** to intercalate with DNA. In contrast to that of [Ru(phen)$_2$dppz]$^{2+}$, the solvent- and temperature-dependence of the luminescence of **3** reveal that the extended ligand aromaticity lowers the energy of the $^3\pi\pi^*$ excited state into competition with the emitting ^{3}MLCT state. Interconversion between these two states plays a significant role in the observed photophysics and accounts for the dual emission in aqueous environments.

These results have key implications to the development of metallo-probes of DNA structure to further enhance our understanding of the subtleties of minor groove association, intercalation, and insertion.[7] As more advanced probes with more specialized steric considerations or further extended π-structures become prevalent, $^3\pi\pi^*$ ligand localized states can mix and compete with the ^{3}MLCT manifold to perturb the excited state dynamics of these probes and lengthen their lifetimes.[50] In some cases, this may not be pragmatically important as rapid equilibrium conditions relative to radiative decay or excited state trapping because of markedly slower equilibration rates with respect to luminescence to the ground state may occur. These conditions can lead to straightforward monoexponential decays that are somewhat invariant across a biological experiment. However, these same rate constants are also solvent environment sensitive, and because of thermodynamic and reorganizational energy considerations, can vary as a function of parameters such as dielectric/co-solvent, temperature, and potentially ionic strength. Therefore it is critical to carefully understand the specific excited state probe dynamics to appropriately interpret binding data from one DNA binding experiment to the next.

Supporting Information Available: X-ray crystallographic data of **3** in CIF format, comparisons of X-ray structure and DFT calculated structure for **3**, resonance Raman spectra of **3** and **4**, experimental Raman frequencies and calculated normal modes for **3** and **4**, DFT molecular orbitals of **1**, TDDFT spin-allowed electronic transitions of **1**, plot of F_1 across the emission spectrum, and Boltzmann plot. This material is available free of charge via the Internet at http://pubs.acs.org.

---

(109) Wang, Z.; Lees, A. J. *Inorg. Chem.* **1993**, *32*, 1493–1501.

(110) Zulu, M. M.; Lees, A. J. *Inorg. Chem.* **1989**, *28*, 85–89.

(111) Kirchhoff, J. R.; Gamache, R. E., Jr.; Blaskie, M. W.; Del Paggio, A. A.; Lengel, R. K.; McMillin, D. R. *Inorg. Chem.* **1983**, *22*, 2380–2384.

(112) Watts, R. J. *Inorg. Chem.* **1981**, *20*, 2302–2306.

(113) Sun, H.; Hoffman, M. Z. *J. Phys. Chem.* **1993**, *97*, 11956–11959.

(114) Caspar, J. V.; Sullivan, B. P.; Kober, E. M.; Meyer, T. J. *Chem. Phys. Lett.* **1982**, *91*, 91–95.

(115) Caspar, J. V.; Meyer, T. J. *J. Am. Chem. Soc.* **1983**, *105*, 5583–5590.